UNIVERSITÀ DEGLI STUDI DI PADOVA

School of Engineering

Department of Information Engineering

Master's Thesis for the degree in

ICT for Internet and multimedia - Ingegneria per le comunicazioni multimediali e Internet

Second cycle degree D.M. 270/2004

Convolutional Neural Networks for Knot Measurement in Tomographic Images of Wood Logs

Advisor: **Prof. Stefano Ghidoni**
Co-Advisor: **Dott. Ing. Enrico Ursella**

Author: **Stefano Giovannini**
Student ID: 1178044

Padua, 7 October 2019

ACADEMIC YEAR 2018-2019

To my parents, for their tireless and unceasing support,
To my friends, who never failed to accompany me in times
both of discouragement and happiness,
To all my relatives who rejoice with me in this day, and to the ones who passed,
To all the people, both older and younger, who entrusted me with a bit of their time
willing to grow together
up to this turning point in my life:

Thank you!

Abstract

In recent years, automation played a crucial role in the development of sawmill industry, especially thanks to the introduction of the first CT scanners dedicated to wood logs.
Such machines allow for the optimization of cutting patterns, therefore contributing to increase final product value, by detecting in advance internal wood defects: knots are the most relevant of these defects, significantly affecting the main mechanical and aesthetic properties of timber Many techniques have been proposed, in the literature, in the field of knot detection and parameter estimation starting from tomographic images: state-of-the-art performances leave, anyway, some room for improvement in terms of knot diameter estimation and Dead Knot Border coordinate regression or, equivalently, knot status determination on single sawn boards. This work proposes novel approaches to tackle such problems by exploiting Convolutional Neural Networks (CNNs). Four procedures are proposed, employing either ground truths obtained from the inspection of CT images or from physical measurements on sawn products. The first two concern the straightforward application of CNNs for parameter estimation and status determination, while the others propose a different procedure, which proves to be more accurate than currently available methods and computationally fast enough to be employed in in-line applications, reaching more than promising results both in terms of diameter regression and status estimation. This approach, concerning the subsequent application of a CNN for status classification to CT voxel sub-blocks containing consecutive portions of each knot, reaches an overall accuracy of 86.5% when tested on a dataset obtained from physical measurements on boards and knot blocks automatically extracted by CT Log.

Contents

List of Figures

List of Tables

Chapter 1

Introduction

Since the early 2000s the global market for wood products has, after a few years of slight decline, steadily kept gaining in volume.
While not holding significant effects in most developing regions of Latin America and Africa, this phenomenon has lead, alongside with environmental concerns and the consequent growth of natural and planted forest areas, to an increase in the availability of raw materials and to the higher request for more diversified and high-quality typologies of product in North America, Europe and some regions of Asia [1].
This trends have been confirmed by the Food and Agriculture Organization of the United Nations (FAO), whose last official reports on the subject show how, by the 2016-2017 biennium, the global volume of production had largely surpassed expectations and predictions carried out barely a decade before [2][3]. All of these factors contribute to the need for better performing machinery and techniques in wood industry and to the consequent development of new technologies aiming to speed up production processes and to improve their efficiency and the quality of final products.
Among the wide variety of commodities the market requests, one of the products having higher demand volume (nearly 460 millions cubic meters as of 2016, [3]) is sawnwood. The sawmill industry offers in turn quite a few typologies of product, many kinds of which are required to have precise properties in terms of quality depending on the intended use, and thus making it one of the principal sectors for what concerns the need and possibility of technological innovation aimed at delivering goods of increasing quality.
Given that the goodness of a product is in greater part determined by the defects of wood composing it, one way to improve the average grading of sawn products is to elaborate accurate models of these defects and to design efficient methods for their estimation, in order to acquire enough information for optimizing the cutting pattern for each log before actually splitting it.
Even though this idea has been rather appealing to researchers and the main industry players in the field for quite a long time, it has proven of difficult implementation because it implies the need for fast and accurate means of acquiring information about the inner defects of wood stems and a noticeable effort towards the improvement of automation techniques in the sawing line.
After a couple of decades of researches on non-destructive methods for log analysis carried out on tomographic images from medical scanners, a milestone in the field was marked by the introduction, in 2008, of the first commercial wood scanner, CT Log by Microtec, which allowed to use Computer Vision algorithms on computerized tomographies of logs to detect

with good speed and precision the main features and defects occurring in stems, such as knots, cracks, resin pockets and the pith (i.e. the center of annual rings) [4][5].
Among all defects, a crucial role in determining the grading of wood products is played by knots, whose status (i.e. the fact they are live or dead when included in a product) can highly affect the quality of a sawn board. In lumber, for instance, the presence of many dead knots could highly affect its mechanical properties, since dead knots may not be adhesive with the surrounding portion of wood and fall out, leaving holes in the board and thus a weak point which makes it unfit for use in construction [6].
Furthermore, since the bigger the size of the knot included in the board, the higher is the effect on the quality of final products, another crucial role for evaluating the precision of a knot model is played by the accuracy with which its diameter is estimated. Unfortunately, gathering accurate information about the diameter and, even more, the status of a knot at its intersection with a specific board in an envisaged cutting pattern proves to be a rather challenging task when starting from tomographic images, mainly because of the difficulty in obtaining datasets from real observations of sawn products for the validation of designed models and algorithms. Current methods, mainly based on segmentation techniques, allowed for only partially satisfactory performances since mainly or, in most cases, wholly focused on the estimation of knot diameter.
Given that they are the de-facto standard in many sectors of Computer Vision, and that several successful architectures have been tested with profit on a wide variety of problems, algorithms exploiting Convolutional Neural Networks (CNNs) have the potential to yield significant improvements with respects to the previously employed techniques, in the case proper datasets for their training are available.
This work has then the objective to design new and better performing techniques for estimating the status of knot intersections with boards belonging to an envisaged cutting pattern and their diameter before sawing, starting from tomographic images and using CNNs.

Chapter 2

Literature review

2.1 Tree biology and wood defects

As common knowledge suggests, the only source for the production of raw wood lays in trees, whose biological structure and growth processes play a crucial role in determining the quality of would-be final sawn products. In order to correctly model and predict defects occurring in wood boards it is therefore necessary to acquire an elementary understanding of natural principles ruling the growth of trees and the formation of those elements resulting in such defects after sawing. The following subsections are thus devoted to a basic description of tree biology.

2.1.1 The structure of trees

Trees are indeed plants, but not all plants can be classified as trees.
A fundamental distinction is the one occurring between woody and non woody plants. The first category, including trees, lianas and shrubs, can be distinguished since exhibiting four main characteristics.
Trees can be defined as woody plants having a single, self-supporting stem, being able to reach an height of at least six meters when fully grown and not generating branches in close proximity of the ground [7].
Woody plants:

- Are *vascular* plants. A woody plant must present conductive tissue articulated in a woody *xylem*, having the role of forming the wood stem and conducting water and dissolved minerals to serve as nutrients, and the *phloem*, acting as a conductor for organic products of photosynthesis (e.g. sugars) and as one of the means to store these resources when produced in surplus.
  In trees, the xylem is the actual woody part, surrounded by the bark, while the phloem is the innermost part of the bark itself. As the tree grows, the part of xylem deputed to conduct sap up the trunk, and therefore having nourishing and food storage functions, looses these capabilities in its central zone, thus giving origin to the distinction between *heartwood* or *duramen* (the central zone) and *sapwood* or *alburnum* (the outer zone under the bark, conserving its original role). When observing a section of a tree,

heartwood and sapwood can, in most species, be easily told apart since the latter has a lighter color due to its greater part of living tissue.

- Are *perennial* plants. A plant can be defined as perennial if its lifespan is greater than an year.
- Have a *persisting stem*. Although being perennial, some plants can't be classified as woody since, even if their roots can survive throughout winter, their stem dies every year. If this doesn't happen, the stem is said to be persisting. In trees, cambium is thus a thin layer placed between wood and bark.
- Present *secondary thickening*. A plant exhibiting secondary thickening has its stem enlarging by subsequent growths in diameter operated by the *cambium* or *cambian*, a growing layer placed between phloem and the most recent layer of wood xylem.

An illustration of the just described layers of a tree trunk can be found in Figure 2.1.

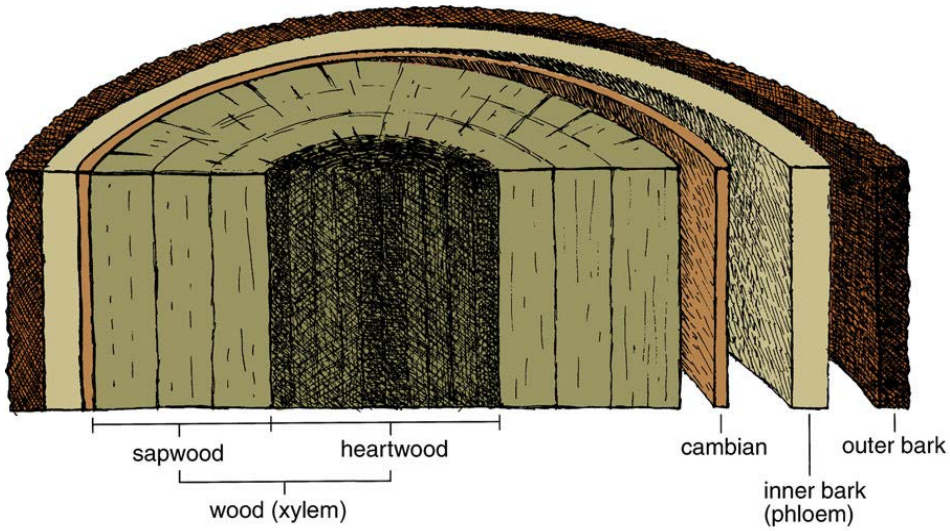

Figure 2.1: All the layers of a tree stem represented in cross-section [8].

Growth by secondary thickening plays a crucial role in determining the principal features of a tree stem, such as its shape, structure and defects.
It works as follows: the thin layer of cambium placed under the bark is actually a generative tissue aimed at producing new vascular cells, which will contribute to increment xylem size on the inner side and phloem size on the outer one.
This phenomenon makes the tree trunk to expand, with approximately radial symmetry, around the *pith*, a small portion of soft vascular tissue that, when the stem is still a twig, has the function of storing and transporting food reserves for the plant. As the tree grows older its cells die, making the pith to loose its nourishing functions. It also stops enlarging in favor of the xylem.
Most species of tree, especially the ones growing in temperate or cold regions, do not grow uniformly during the year, but alternate some periods of expansion (in spring and summer) with others where there is no growth. When observing the section of a tree cut in parallel to the ground, it is possible to observe *annual rings*, marking the points in which the tree stopped growing approximately each year. According to how the tree is sawn after felling, annual rings give origin to a specific pattern of wood-cell fibers lines on each board (highly

contributing to structural properties in lumber), taking the name of *grain*.
While newer layers of wood encase older ones by secondary thickening (or growth), the tree also gets taller by primary growth, which can be described in short as the process of elongation of branches and tree top. The combination of the two gives the plant a cone-like shape, since older, lower parts of the tree are covered by more layers of new wood (approximately one every year) and the ones further up on the trunk are thinner, since originated in subsequent years (see Figure 2.2) [7][8][9].

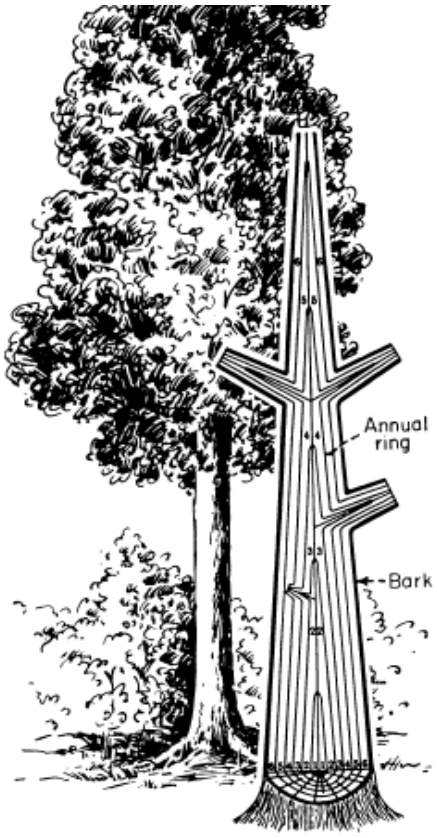

Figure 2.2: Longitudinal section of a tree showing the yearly growing pattern [9].

The understanding of this growth pattern proves useful to describe the nature of some of the principal wood defects occurring in sawn boards, as explained in the following subsection.

2.1.2 Principal wood defects

After the process of sawing, wood boards unavoidably end up presenting some features labeled as defects.
A defect can be defined as an irregularity in wood pattern that affects its quality in some way, being it by weakening some mechanical property (e.g. strength) or by spoiling its appearance, therefore decreasing final product value.
Wood defects occur in many ways, and no kind of wood or wood product is exempt from their presence. Certain are peculiar, or at least more frequent, in some species of trees, while others are common to all: some imperfections are inherent to the very biological processes ruling the growth of trees, such as knots, some are due to environmental conditions the plant was exposed to during its lifespan and some are due to the intervention of foreign organisms (e.g.

bugs).
The following subsections report a list of the most common or relevant defects in wood as described in [7] and [10]. Only the description of defects having a role in the prosecution of this work is reported.

Knots

As the tree grows, buds originate new twigs along the stem in proximity of the pith, thus starting the creation of new branches.
Having their own pith and vascular tissue, new twigs grow towards the outer border of the trunk with the exact same modalities in which the tree itself grows: branches too, in fact, get longer by primary growth and thicker by secondary growth.
The layer of cambium in branches is, during their period of growth, actually a continuous extension of the one belonging to the main plant, meaning that, as new portions of the xylem are formed, the oldest part of the branch gets smoothly encased in the trunk, since its cambium on the inner side becomes actual wood, and not bark.
A neat distinction between wood from the main trunk and the encased branch is, in any case, clearly visible when observing sawn logs. A (portion of) branch embedded in the wood of a tree trunk can be defined as a knot.

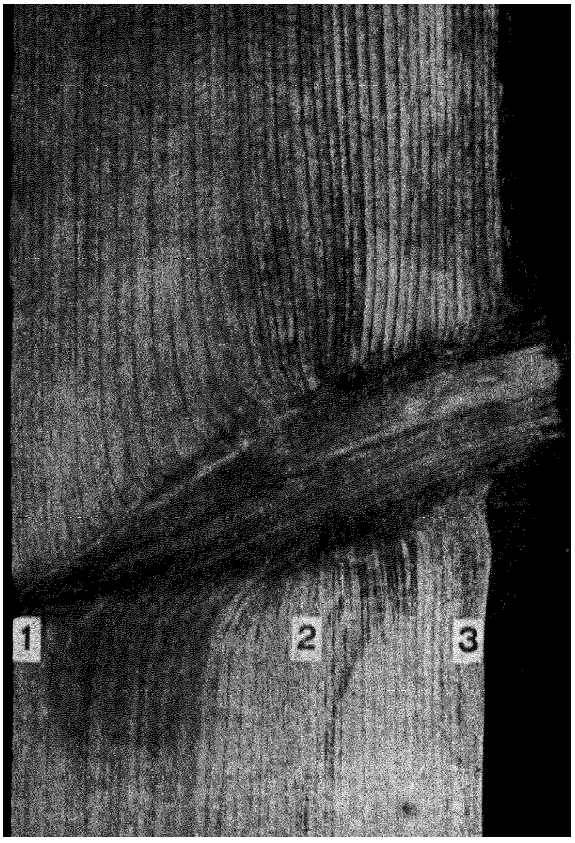

Figure 2.3: Section of a *Pinus Strobus* knot [7].

The previous figure, reporting the vertical cross section of a *Pinus Strobus* log, permits to understand how knot growth happens: between mark 1 and 2 it is clearly visible (especially on the upper part) how fibers in along the vertical direction of the xylem seamlessly bend towards the axis of the knot and generate a quite smooth transition from trunk to branch.

In the area comprised between 2 and 3, however, a more marked transition can be observed. This happens because, at a certain moment in the life of the tree, branches (especially the older ones, closer to the ground) die and stop growing by secondary growth. For a while the branch keeps elongating, but its cambium layer gets disconnected from the main one on the trunk edge, and develops its own bark. After some time, depending on the species, it is cast by a natural phenomenon known as *cladoptosis* or breaks and falls (natural pruning).
As the stem widens by secondary growth, this later portion of branch is gradually incorporated into the main body.
When looking at a knot, its dead part can be easily spotted since wood fibers surrounding it do not bend to follow its growing direction as for its previous segment and a thin layer of bark is clearly visible around its borders. The portion of knot ranging from 1 to 2 is said to be *sound*, while the one comprised between 2 and 3 is defined as *dead* or *black*. Point 2 is also known as the *Dead Knot Border* (DKB).
On sawn boards knots can be either *spike* or *round*: spike knots occur when the outer surface of the board is approximately parallel to their growth direction, as in the case of Figure 2.3, while round knots are generated by almost orthogonal cutting angles and present circular to oval shapes. Spike knots, except in the case of wholly sound knots at the moment of tree felling, nearly always present both a black and a sound part, but round knots most often belong to either one of them.
On lumber, having a dead knot is not a desirable property, since, being it not tightly adherent to the surrounding wood or even surrounded by its own layer of bark, such knot is likely to detach and leave a *knothole* behind, which weakens the product and thus affects its mechanical properties. Moreover, dead knots are an aesthetic defect, their presence being undesired in lumber employed for the construction of products in which visual aspect determines a considerable share of the final selling price.
Figure 2.4 reports an both an instance of sound and black round knots.

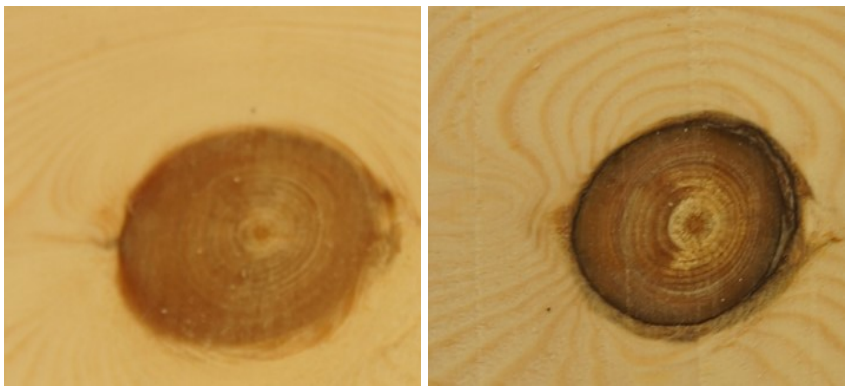

(a) An instance of sound knot. **(b)** An instance of dead knot.

Figure 2.4: Examples of round knots.

While both knots create a noticeable discontinuity with respect to the rest of the board, the one on the right blends less smoothly, with the surrounding wood grain stopping abruptly on its border. Moreover, its color is darker, hence the definition of black knot, and it is encircled by a clearly visible layer of bark.

(a) Compression wood (bottom left of the log).

(b) Lumber with rot (red stains) [11].

(c) A pitch pocket.

(d) Spiral grain on a board.

Figure 2.5: Examples of wood defects.

Compression wood

As previously stated, the environment surrounding a tree during its growth is one of the main sources of wood defects. If the plant, in its first period of life, is forced to lean (e.g. because it is growing on a slope) an abnormality in the development of its wood tissue known as *reaction wood* may occur. Depending on the species of tree on which it is found, it takes two different names: *tension wood* in hardwoods and *compression wood* in conifers (the distinction between hardwoods and softwoods, or conifers, is dictated by the different ways in which they manage leaves and nourishing, which is out of the scope of this work).
Being the result of longitudinal stresses in the wood due to tree inclination, reaction wood generates, as the names suggest, from compression on the underside of the leaning point of the trunk in conifers and from tension in upper parts, with respect to where the tree bends, in hardwoods. Since the near totality of the examples reported in the following regards conifers, only the term compression wood will be hereafter used.
Visually, compression wood can be identified as a redder or generally darker portion of the trunk with a lifeless appearance.

Rot

Also known as *decay*, rot is the decomposition, eventually resulting in the breakdown, of wood composing a log or board.
A continuing process, it starts by the action of some species of *fungus* or micro-organisms: in initial phases it makes wood slightly softer and weaker, but not enough to make it unfit for construction or any other use. After this early stage, in which the defect may even go unnoticed to an observer, rot progresses up to a point when the affected wood looses its structure and leaves a hollow.
It may affect both heartwood and sapwood areas of the xylem.

Pitch pockets

Pitch pockets are a defect common to species where resin canals can be found in wood, such as pine, spruce and fir, but they can also develop in any conifer after an injury occurred to the cambium layer.
They are small cavities convex on one side, usually contained inside the wood limited by two annual rings, with the convexity pointing outwards. Appearing as ellipses with the major axis laying parallel to the direction of the grain, they can either be empty or contain liquid or solidified resin. They may even present small portions of bark, included during their formation. The dimension of a pitch pocket along the principal axis of the oval can span a few centimeters.

Cross graining

Because of the irregularity of tree growth due to environmental or genetic factors, age rings are never equal to one another. Different inclinations and sizes with which they form give origin, after cutting the tree into lumber, to a phenomenon on boards defined as *cross-graining*, consisting in a deviation of grain from the vertical axis.
Although it can be introduced by errors in the cut (e.g. extraction of a non perfectly vertical board from the log, known as *diagonal grain*), it is a mostly natural defect taking the name of *spiral grain*: when debarking a log, its appearance may seem twisted because its grain follows a spiral pattern around the trunk. This effect is more accentuated close to the base of the tree, while tends to get weaker going up the stem, with an usual change in the direction of the spiraling at the height reached by the tree between 10 and 30 years of age.
Its supposed purpose concerns the enforcement of the trunk against atmospheric agents and food distribution functions [8].

2.2 The role of defects in product quality

The concept of "quality", when linked to the determination of a value for wood products, is inherently relative to the intended use of the product itself.
When it comes to purely aesthetic factors, defects such as spiral grain or knots of considerable size may happen to be, if not explicitly wanted, at least accepted.
By "quality" it will be hereafter meant the possession, on part of the board, of certain of the mostly required mechanical properties in lumber, such as elasticity, strength (e.g. resistance to bending, tension and compression) and torsion strength [12].
Defects can therefore be re-defined as all those imperfections, meant as deviations from an

ideal, perfectly cylindrical tree trunk wholly made of perfect and uniform wood, responsible for lowering final product quality. More specifically, defects treated in this section are *grade* defects, i.e. all the imperfections reducing a log or sawn product quality, that can not be removed by just discarding a fraction of the considered material, to be distinguished from *scalable* defects, such as rot, that can most often be so eliminated [10].

2.2.1 Grain angle

Quite a few studies (see, for instance, [12] and [13]) have proven the anisotropy of timber with respect to tension, compression and bending strength, i.e. its resistance to those operations is directionally dependent. More specifically, the two aforementioned studies refer to some experiments performed on test pieces of Douglas Fir, clear of any relevant defect and therefore exhibiting no angle between the directions of tree growth and grain.
Results are clear: in straightly-grained timber resistance to tension has proven to be approximately 48 times higher in the direction parallel to tree growth than in its perpendicular and 6 to 7 times for compression. In absence of relevant defects, timber is thus more resistant to tensile strength than to compression and its resistance to stress is strongly dependent on the angle at which the perturbation is applied (the more this force is parallel to tree growth direction, the more resistance wood offers).
These properties are guaranteed by the presence of straight grain, since it is its cellular structure to provide them: this implies that resistance of timber to compression and tension is actually dependent on the angle of application with respect to the grain.
Therefore, in case of cross graining, timber boards are less tolerant to compression strengths applied along their main two axes since they are forming an angle greater than zero with the grain. Similar results are obtained for bending strength.
Figure 2.6 shows how resistance to compression, tension and bending strengths decreases in function of the angle at which it is applied with respect to the grain. With slightly different patterns, resistance to all three strengths suffers steep decreases starting from angles of 15-20° and reaches 10-20% of its maximum around 60°. A more complete series of results on the effect of grain angle on mechanical properties can be found in [12].

2.2.2 The effect of knots

Under the light of what reported in the previous subsection, any defect on timber affecting parallelism between grain and main axis of the board weakens its mechanical properties.
Since, as can be seen in figure 2.3, knots can cause strong deviations in grain direction along their sound portion or even its abrupt interruption in the dead one, they are a considerable source of weakening in sawn boards. The importance of the role they play in degrading quality depends, anyway, from their sizes and distribution along the product, since bigger knots have greater influence than smaller ones and clusters have more detrimental effects than single instances. Moreover, even their position is relevant since different portions of a product can be subject to different kinds of stress: taking, for instance, a simple timber beam with some load applied on the top: if on the upper side, knots would be more subject to compression strengths, while tensile ones would play the major role on the lower side [12].
Many studies have been conducted on the subject, and the role played by knots in weakening lumber has been long known, with many articles published in the last seventy years. Many of them focused on the principal role played by knots in the introduction of grain deviation,

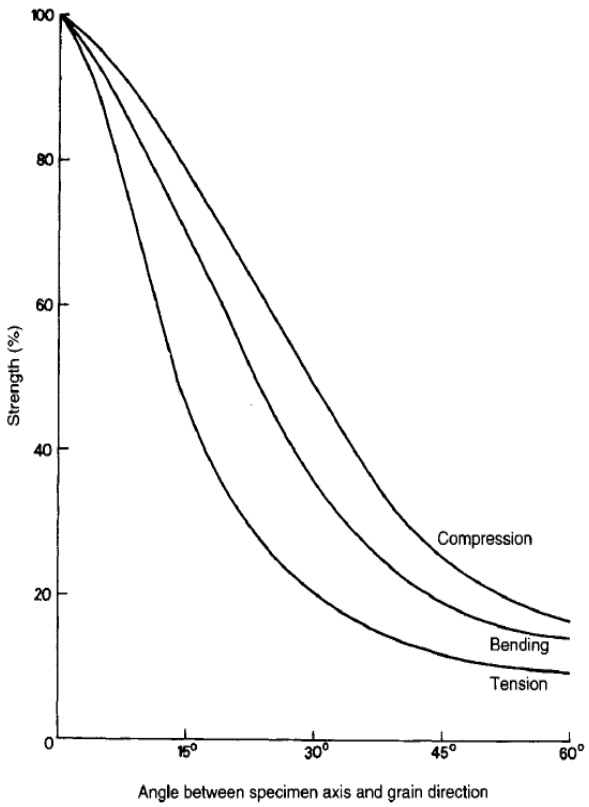

Figure 2.6: Effects of some strengths on timber, depending on grain angle [14]

while others analyzed other side effects of their presence, such as the inevitable reduction of clear-wood areas, the redistribution of stresses around in the surrounding portion of material and their close-to-null tensile strength resistance. Moreover, according to [15], the presence of a knot causes grain deviation in a zone approximately as large as three times its diameter. Although sound knots introduce the same effects of grain deviation in a more quality-degrading fashion, their detrimental effects is surpassed by the ones caused by dead ones, which can be in full modeled as holes with undisturbed surrounding fiber directions. These holes serve as concentration points for stresses and thus highly affect overall product quality. A good summary of the principal studies in this regards can be found in [14].
A quantitative analysis about the influence of knots and grain deviation on the resistance of timber to bending, tensile and compression strengths was conducted in [13] on some species of spruce, pine and fir. Its results are reported in the following Table 2.1.

Timber	Tension [N/mm^2]	Compression [N/mm^2]
Sitka spruce	19.7	29.5
Douglas fir	21.4	32.1
Canadian spruce/pine/fir	26.3	39.5
Norway spruce	30.5	45.8

Table 2.1: Resistance to tension and compression for some tree species.

It is possible to notice how, for each and every one of the tested species, the mean value of tensile stress resistance is lower than the one of compression. Furthermore, in the case of Douglas fir, a direct comparison with what reported in subsection 2.2.1 is possible: in the case of straight-grained timber without knots, resistance to compression proved to be 7 to 8 times smaller than the one to tension, while the presence of defects leads it to be 1.5 times bigger. Further results are, one again, reported in [12].
In addition, some studies (see, for instance, [14] and [16]) assert that, although the main role in strength reduction is played by fiber deviations, in boards where large knots are present they become the most important factor affecting grain orientation and therefore overall strength.
In particular, [14] proves that, although a major role in the decreasing of lumber stiffness is played by material variations of clear wood or the presence of natural defects, such as compression wood, which is particularly difficult to quantify, the part played by knots is still greatly relevant and the effect of their presence is not correlated to these natural defects, therefore meaning that their influence on stiffness reduction can be estimated without precise knowledge of material variations inside the board. This implies that, with a fair approximation, knots alone can even be used to estimate strength and behavior of lumber.
It is therefore clear that knot distribution, sizes and status (sound/dead) play a crucial role in determining mechanical properties, and therefore overall quality, of sawn boards.

2.3 Tomographic images in sawing optimization

During the years, alongside the development of research and market, new and more accurate product grading standards have been developed, also including guidelines for machine grading, which has been gaining ground over plain visual board grading in the last period.
Scanners are nowadays capable of evaluating the quality of boards by considering several factors, such as dimensions, knots, slope of grain compression wood, presence of bark or damages and others, thus allowing for a speedup in production and efficiency.
Examples of grading standards and scanners performing their evaluation can be found, for instance, in [16], [17] and [18].
Anyway, quality evaluation performed on boards is bounded to have a limited contribution in increasing the value of final products, since it is unavoidably performed after the log has been split into lumber. Moreover, without any external aid, the choice of sawing pattern solely relies on the experience of sawyers or sawing machine operators. This often results in non-optimal cut choices and a sensible decrease, with respect to the optimum, in product grade and even volume, in case an erroneous choice in sawing results in discarding entire portions of the log.
Although, since the 80s, some optical scanners were used to gain information about log geometry in order to maximize product volume yield, several studies have shown that a major increment in value would be guaranteed by an accurate knowledge of defects positioning before cut, thus allowing to optimize log rotation angle and sawing pattern.
As reported in [19], a milestone in modern sawing optimization, achieving a close-to-optimal log rotation before log splitting can yield an average of 7% improvement in resulting lumber value, while improving the cutting pattern by considering the placement of internal knots could lead to a 12.7% increase in top-grade lumber extraction.
Other studies of the same period confirmed the noticeable grade and value increase achievable with the optimization of log rotation with respect to the principal defects, up to the point of stating that they should play the principal role in a sawyer's decision of log positioning before the cut.

2.3.1 Towards the use of tomographic images

After a few years from the introduction of commercial Computerized Tomography (CT) in 1972, it started drawing the attention of the sawmill industry, since the chemical composition of wood carbon chains allowed to obtain outputs not very different, in quality, from the ones obtained by its application in medicine, thus paving the way to the analysis of the internal structure of logs prior to sawing.
One of the first important publications was the already cited one from Taylor et al. ([19]), a feasibility study on the use of CT images for analyzing knots inside uncut logs. The study, employing a basic segmentation technique based on thresholding, was the first to prove the feasibility of defect recognition (and, more specifically, knot recognition) starting from tomographic images. Other important works soon followed, such as [20], which confirmed the accuracy of defect detection algorithms operating on CT images, but were still far from working fast enough for sawing lines.
These first studies, anyway, were bounded to the mere detection of knots, which was indeed a noticeable improvement with respect to contemporary sawing techniques, but lacked for a more accurate description of such defects needed in order to further increase the projected grading, and thus value, of final products. A natural extension of these studies pointed therefore in the direction of a more accurate prediction of the specific structure of defects present in the log, in order to gain fundamental information for a considerable improvement in sawing patterns.
Given the objectives of this work, the following sections and chapters will be entirely focused on knots, which are the most common grade and value reducing defect present in lumber coming from many species of tree. The attention will be especially placed to the estimation of some fundamental knot parameters, discussed in the following, which allow for an accurate description of the defects needed to optimize cutting choices.

2.3.2 Knot modeling and measurement

In order to properly estimate the impact of knots on the grading of boards resulting from sawing, according to a chosen cutting pattern, it is necessary to know their size at a given position and whether, in that very spot, they are sound or dead. This can be done via a proper modeling of knots by defining some parameters.
Before proceeding with a brief description of the most important knot parameters having a role in knot modeling, it is necessary to define a reference system for log and knots. From here on, the longitudinal (l) direction of the log will be the vertical one following tree growth, the radial direction (r) will be the one running parallel to log radius (i.e. perpendicular to knot radius), while transversal (t) direction will be perpendicular to it.
Some of the most important knot parameters are:

- *Starting point*. It is the point where the knot originates, the innermost and closest to log center. Since it most often resides in the pith, it is itself known by "pith". When dealing with knot models it is most often chosen as the origin point for the reference system, thus meaning that all its r, t and l coordinates are equal to 0.

- *Knot end*. As the name suggests, it is the ending point of the knot. If the knot dies at a certain point, it is most likely to occur inside the log, while it is on log surface for sound knots or knots which stopped growing in its close proximity (i.e. its part reaching log edge is made up of dead wood).

- *Length*. It coincides with the radial distance of knot end from the pith.
  For a sound knot reaching the edge of the trunk, it indeed coincides with log radius along the direction marked by knot growth. In some cases a sound knot may happen to be pruned by man or accidentally broken: this truncation affects its end point (and therefore its length) and has a detrimental effect with respect to the accuracy of knot detection in tomographic images since, because of irregularities in the process, branch end assumes an irregular shape known as *scar*.

- *Diameter*. At a given radial coordinate, it is the maximum width of the knot in the rt-plane. When referring to knot diameter, it is the maximum diameter along the radial direction.

- *Dead Knot Border* (DKB). Radial coordinate at which the transition from sound to black knot takes place. Knots reaching log border without changing state (therefore globally labeled as sound) do not indeed exhibit one.

The following Figure shows the projection of a knot on a single cross-section along the l axis and reports a representation of the parameters described above. DKB and (knot) diameter are represented in two separate lines for the sake of clarity, even though many models make them coincide.

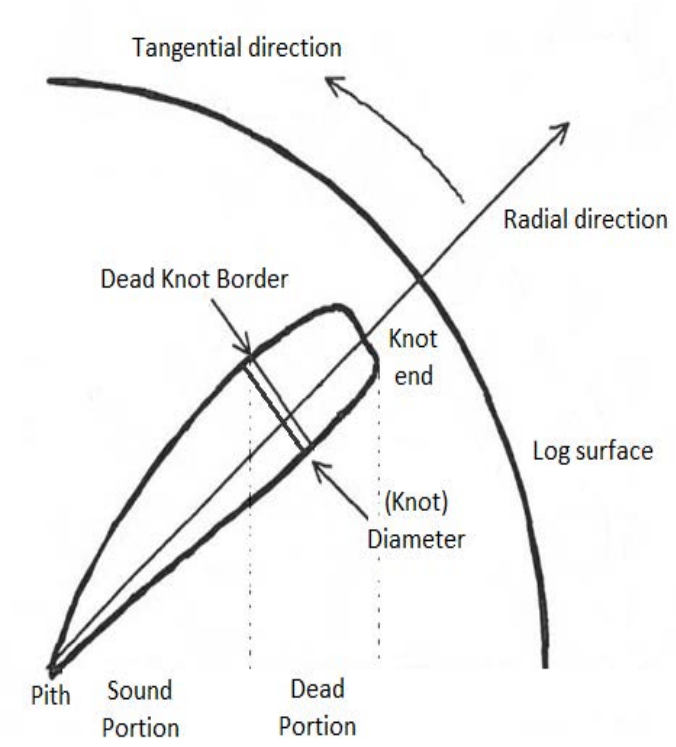

Figure 2.7: Representation of principal knot parameters. Original image from [21].

Some models developed in the literature also provide mathematical relations between these parameters. An instance of them can be found in [22], but the most important and validated of these models is the one designed by Grundberg et al. in 1995 ([23]), improved and validated by Oja in [24] and Grundberg and Grönlund in [21].
Developed for Scots pine and refined on Norway spruce samples, this model utilizes a set of

nine parameters (among which there are knot length, DKB coordinate and the distance from pith to log surface along the radial direction) which have to be obtained from (manual or automatic) measurements and allow to obtain, as their function, the transversal and longitudinal positioning of knot axis and knot diameter at any radial coordinate.
Such a model turns out to be of particular interest since its parameters could be obtained by automatic analysis of CT images, especially in the case of diameter and DKB, which instead of being measured could be defined as the radial coordinate at which the diameter stops growing.
The previously cited papers, with some others, provide a measure of the accuracy with which the mentioned model predicts actual knot shape and features starting from CT images. Here follows a brief summary.

2.3.3 Destructive methods: creating a ground truth

In order to obtain some physical knot measurements to serve as ground truth to validate any kind of model or algorithm it is unavoidable to perform the breakdown of the log (hence the name "destructive") and manually measure the quantities of interest. There are several ways of doing so: only two of them, specifically the ones used by Oja to validate the model from [23], are here reported.
A first and more lengthy method (Figure 2.8a), but also more precise, makes use of knot whorls, that is a group of knots whose starting points are placed all around the pith, but in a short interval along the longitudinal axis, since coming from branches originated approximately in the same period. This method consists in spotting whorls along the log, and then cut right above them. Successively each single knot is isolated, split along its center and measured.
Another method (Figure 2.8b) consists in longitudinally splitting the log into flitches, also referred to as boards, of a certain width (20 *mm* in the case of Oja's study), then manually scanning each board and annotating position, dimension and status for each knot.

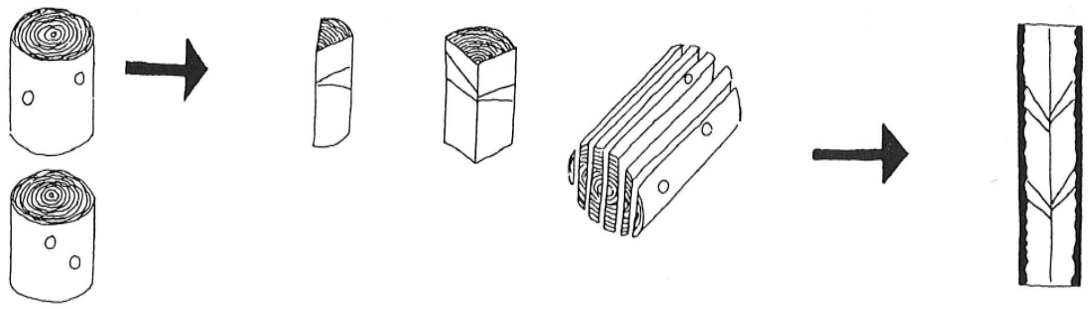

(a) Method exploiting whorls. **(b)** Splitting a log into flitches.

Figure 2.8: Destructive methods for knot measurement [24].

Although the first method proves to be more cumbersome, it also allows for way more accurate measurement of fundamental knot parameters such as length, DKB and diameter with respect to any other, even though some knots are unavoidably lost in the process, since splitting the log in correspondence of very small knots proves to be very prone to errors that can compromise final measurements. Sawing the log into boards, on the other hand, allows for the gathering of measurements about approximately every knot, but gives very imprecise information about knot length, diameter and DKB, since only a few samples for every knots

are available, i.e. the points where they intersect a board, therefore allowing to obtain only sparse measurements (except in the case of spike knots). This method was also employed in the construction of one of the most important and cited databases, the Swedish Pine Stem Bank, whose structure is described in [23], the original 1995 paper in Swedish and in [21].
The Stem Bank originally included 200 Scots Pine stems coming from all over Sweden, some of which had been studied for up to a century, and was later on extended to include more samples. CT images were gathered for all of them, by using a medical scanner by Siemens, the SOMATOM AR.T., with a precision of 10 *mm* along the longitudinal axis in correspondence of the whorls and 40 *mm* between them.
Logs were then split into boards and each board marked for allowing to reconstruct its position in the original log. After they were scanned with cameras on all sides, two experts then analyzed and graded each board.

2.3.4 Using CT images for knot detection and measurement

Preliminary studies

In his test, Oja compares measurements from ground-truths obtained with the two aforementioned destructive methods with results coming from the analysis of CT images via basic thresholding techniques. Information obtained via the whorl method is assumed to be the correct one, since the measurements of knot key parameters is, by construction, more precise.
While being accurate in determining knot position, measurements performed on CT images overestimate knot diameter, with a mean error of 2.6 *mm* and a standard deviation (std) of 2.2 *mm*. The error is quite bigger for DKB, with a 15 *mm* mean and a 18 *mm* std.
Oja explains these not very satisfactory results in terms of DKB position estimation as obtained from a probably insufficient number of samples, as possibly affected by the drying of logs, which can alter knot structure and therefore their parameters, and, mostly, as coming from the application of an inaccurate model. The model in question, previously mentioned in subsection 2.3.1, is designed on Scots pine knots and determines as DKB coordinate the one at which maximum knot diameter is reached: this, Oja states, is not true for the Norway spruce knots object of his study, whose different geometry does not give a distinct maximum diameter in CT images.
Grundberg and Grönlund adopt a different technique in [21]: CT acquisition of logs from the Swedish Stem Bank are simulated by applying a mathematical model of X-ray tube and detector and the same knot model is applied on images processed basing on density levels, variations and shapes. Adopted metrics for performance evaluation are different from the one used by Oja: on 539 knot observations the dead knot *volume* per considered whorl is predicted with an R^2 of 0.81, while knot diameter had an R^2 of 0.66.
Although performed on simulated data, this study contributed to prove the goodness, in perspective, of the application of CT image analysis to sawing optimization, but also remarked the difficulty in obtaining a proper estimation of some fundamental knot parameters.

A closer look to CT images of logs

Some of the methods and algorithms available in the literature and dealing with knots work on the full three-dimensional log tomography, while others just analyze small portions of consecutive 2D slices.
Log tomographies can be considered as a set of bi-dimensional images stacked along the

longitudinal direction of the stem, which are also referred to as "slices". An example can be

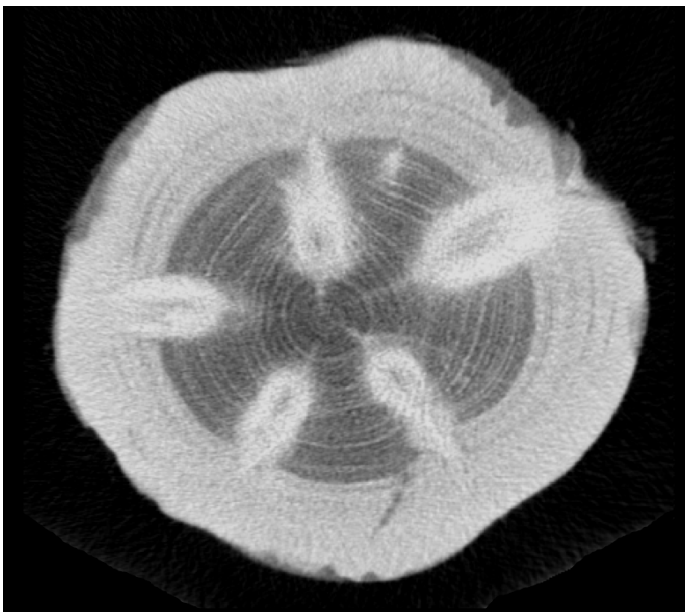

Figure 2.9: A CT slice from a Scots pine log.

found in Figure 2.9, where it is also possible to notice five knots composing a whorl, clearly distinguishable as lighter zones with an approximately elliptical shape around which age rings slightly bend towards the outside of the log.
The distinction between heartwood and sapwood is also clear: the former is the darker zone in the middle where (in this specific image) most part of the knots resides, while the latter is the outermost, brighter part. It is important to notice that the difference in density between knots and sapwood, reflected in image color, is not very marked: this is a well known problem in the literature, with some studies entirely devoted to it, such as [25].
The resolution of a single slice (in the order of $1mm$ x $1mm$) is usually quite higher than the one between consecutive slices (up to the order of the centimeter), therefore nearly all the algorithms presented in the literature are designed to work on slices rather than longitudinally.
The slice reported in Figure 2.9 was taken from the scan of a Scots pine log performed with CT Log by Microtec [4], the scanner employed for this thesis, treated in the following of this work.

State-of-the art techniques for knot detection and measurement

In more recent years, several other studies concerning knot modeling and parameter estimation starting from tomographic images have been carried on. While preceding ones were only feasibility studies aiming to prove the effectiveness of using CT images for sawing optimization, these latter publications are also focused towards the problem of performing automatic knot detection. The role of this task is fundamental in industrial applications, since it is the preliminary step for knot parameter estimation and sawing optimization.
Quite a few papers deal with the subject, an example of which is [26], by Andreu et Rinnhofer, proposing a knot detection method based on histogram thresholding of consecutive CT slices of Norway spruce (with a 20 mm resolution along the l axis), preceded by some pre-processing steps, such as sapwood segmentation aimed at isolating knot surface from the rest of the log. Extracted shapes in consecutive images are reported to a mathematical model based on fitting

the knot around a three-dimensional spine. This method allows to correctly extract 73% of knots with a 13% of false alarms. The employed model also allows for diameter estimation with a mean error of 0.7 *mm* and a std of 10.1 *mm* with respect to a ground truth obtained by destructive measurements.
Another method exploiting 3D knot connected components among successive slices is proposed by Longuetaud et al. in [27], reaching a 85% detection rate.
Although its results concerning maximal knot diameter estimation appear to be very satisfactory (approximately 0 *mm* for mean and 0.9 *mm* std), they were obtained with respect to measurements carried out by marking the ground truth directly on CT images via a computer software, thus not on physical boards or log sections (notice that actual knots may be different in size from their CT scansion, either because of a limited resolution or imperfect image reconstruction), and were not tested on an independent validation sample, thus being of difficult comparison with other studies.
In [28] the authors choose to perform a direct comparison between knots in CT images and on physical cross-sections of logs, therefore not considering any three-dimensional knot structure or model. Each knot is isolated as follows: every image is centered around the pith, then heartwood-sapwood boundary is detected in order to eliminate the sapwood part, which could affect performances in knot detection. Eventually each knot is segmented by gray level thresholding with a fixed-value threshold and rotated to be aligned with the vertical direction, in order to reproduce the scheme employed in manual diameter measurement, which was performed on physical cross-sections of Norway spruce logs, with three diameter samples for each knot.
Error mean (1.7 *mm*) and especially std (4 *mm*) in diameter measurement are good results if compared with other studies employing physical measurements on boards as ground truth. The authors do anyway point out the fact that manual measurements could have an uncertainty up to 5 *mm* in some cases, especially in presence of big sound knots, many of which exhibit only a faint color transition to the surrounding wood and prove tricky to be measured with high accuracy even by an expert.
The different, previously mentioned study by Longuetaud et al. ([25]), employed a similar ground truth, and achieved on diameter measurement a mean error of 0.67 *mm* and a root mean squared error (rmse) of 3.28 *mm*.
Cool et al, in [29], perform an interesting study aimed at measuring knot detection and parameter estimation performances starting from coarse resolution CT images to simulate the effect of an high speed industrial scanner. Using four logs from three different North-American tree species, they apply the algorithm from Johansson et al. [30], reported further on in this section, on 146 x 146 pixel images and compare its results on a ground truth created by manual measurements on CT images. The obtained results (-3 *mm* mean error, 7.2 *mm* std) are, anyway, not fully satisfactory and show how knot measurement proves to be a difficult task with a degraded resolution of CT images.
In [31] the authors test the same algorithm on a set of partially dried logs (therefore exhibiting different sapwood properties, which are reflected in CT images by means of an altered hardwood-sapwood border) with knots once again measured directly on tomographic images. The tests yield a -1.87 *mm* mean error and a 4.87 *mm* std.

The issue of Dead Knot Border

All the literature reported up to now is mainly focused on the issue of evaluating the effectiveness of the CT approach in detecting knots and evaluating some of their principal parameters

having a role in product grading and value. Anyway, the near totality of the available studies does not provide any result in terms of DKB position estimation.
This lack is, in any case, motivated by some objective difficulties, first of which the one concerning the creation of a dataset large enough to guarantee the reliability of obtained results. This happens since DKB is only measurable when viewing a knot in its whole, or at least its section along the radial direction: it's the case of a spike knot on a board, which can be obtained with destructive measurements both in the flitch method and in the whorl one. But it must be noticed that the former is performed without any knowledge of internal knot disposition and results in a random fraction of spike knots in the obtained boards, while the latter, although allowing for a more accurate split of nearly each knot present in a whorl, is very time consuming, requiring approximately 5 hours of work per log and the hand of a skilled expert.
Moreover, methods only exploiting CT information and considering the DKB as the point where knot diameter stops increasing are inherently imprecise, since the determination of such a point is hardly ever univocal and is rather prone to judgment errors.
Some few works reporting results about DKB position estimation are, anyway, allowable in the literature, among which are noticeable another study by Oja [32], dating back to 2000 and the one by Johansson et al. [30], published in 2013.
The algorithm designed in [30] and employed in some of the papers cited above (but only now discussed to serve as direct comparison with Oja's) works by employing concentric surfaces (CSs) centered, in each slice, around the pith: these surfaces do not have a fixed, circular shape, but can follow either the shape of heartwood-sapwood border or log exterior shape. In three dimensions, these surfaces extend to close-to-cylindrical shells intersecting the log (and therefore its knots) at a certain distance from the pith.
On the slice plane, each knot portion comprised by two surfaces, isolated by a thresholding operation, is roughly approximated with an ellipse: since ten CS are employed (5 in heartwood and 5 in sapwood) nine ellipses are fit to knot portions. A whole knot is then formed by joining them and its shape refined, especially in sapwood where it tends to be confused with the surrounding portion of log, by morphological dilation. Eventually knots are fit to the model designed in [23], with the DKB set to be the coordinate in which diameter reaches its maximum.
This procedure, tested on a mixed ground truth of pine and spruce coming from the Swedish Stem Bank reached a mean error, for diameter estimation, of -0.93 *mm* (4.6 *mm* for std) on pine and of 0.93 *mm* (5.1 *mm* for std) on spruce.
Results on DKB are only available for pine, and report a mean error of -4 *mm*, with a std of 12 *mm*. Measured R^2 is equal to 0.19.
In [32], Oja follows a different approach: while adopting the same procedure of his previous work ([24]), he validates it on a wider sample of Norway spruce in the process of being added to the Swedish stem bank, therefore guaranteeing a higher reliability on the ground truth results are tested against.
Once knots are detected and their parameters measured by the algorithm, virtual boards are created according to these measurements and the original cutting pattern with which logs constituting the ground truth were split. These reconstructed boards are then compared with the scansion (via CCD line camera) of original ones, so allowing to evaluate the performances on any single board, thus globally obtaining more than one measurement per knot and increasing dataset dimension.
Knot diameter was evaluated only on samples whose ground truth was a spike knot, thus

allowing for the contemporary identification of maximum diameter and DKB as the coordinate at which it is reached. Only 27 of these knots were found on sawn boards, resulting in a prediction with mean error of -2 *mm* and std 3 *mm*.
Although DKB was estimated for every knot in the model, only the results relative to 12 boards are reported in the paper. Since knowing the DKB position allows to assert the state of a knot on a sawn board intersecting it at a certain position, a possible metric for evaluating the performances of its prediction is the share of sound knots on a single board correctly labeled so by the algorithm. In the article only the accuracy on boards with more than 30% of sound knots in the ground truth is reported, while it is stated that the algorithm fails on wider logs with a majority of small, dead knots since trunk width allows for a weaker x-ray penetration and thus a lower resolution in CT images, resulting in poorer performances.
The image reporting Oja's results can be found in Figure 2.10.
Only real knots (i.e. belonging to the ground truth) found on innermost, central boards of the cutting pattern and placed on its their sapwood-facing side are considered.
The abscissa represents the share of sound knots of the reconstructed board generated by the data provided by the algorithm, while the ordinate corresponds to its ground-truth equivalent. The coefficient of determination of the linear regression is measured to be $R^2 = 0.72$.

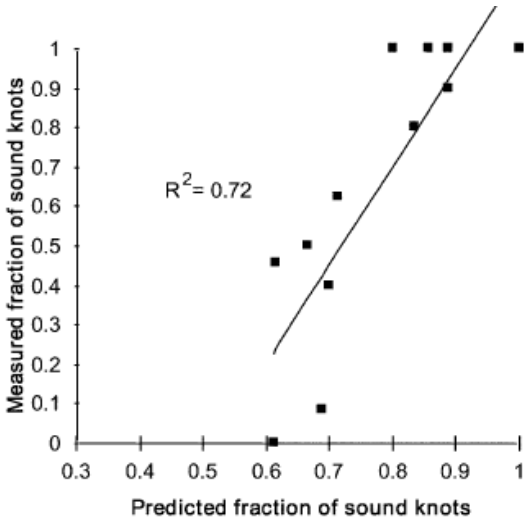

Figure 2.10: Results on DKB prediction by Oja [32].

Summary

In the course of this subsection several methods and results concerning knot parameter measurement starting from tomographic images were presented. Two main possible choices for ground truth creation were introduced: one involving parameter estimation directly from the same CT images against which algorithms and techniques are tested and the other employing destructive methods on logs, after the tomographic scansion has been performed, to obtain accurate measurements directly on wood.
Moreover, some of the most relevant paper on the subject were briefly discussed. Table 2.2 reports the only couple of available results in terms of DKB estimation.
It is immediate to notice that these result, even if obtained with CT images coming from the same scanner, are not of easy comparison since completely different metrics are adopted, i.e. actual error with respect to ground truth measurements in the case of Johansson et al. and

Paper	Performance
Johansson et al. [30]	mean error = $-4mm$, std = $12mm$
Oja [32]	$R^2 = 0.72$

Table 2.2: Comparison between performances on DKB estimation.

coefficient of determination of the linear regression between the share of actual and predicted sound samples on a board for Oja.
Table 2.3 reports instead the results on knot radius estimation. Even though in this case they are of easier comparison, performances are here split in two main groups: those obtained from measurements operate on CT images (the first four) and those evaluated on a ground truth obtained from a destructive method.
Scanner resolution is also reported for completeness of information: the first two numbers indicate horizontal and vertical resolution for each CT slice, while the third stands for the resolution along the longitudinal axis.
Results reporting rmse instead of std are marked with an asterisk (*)

Paper	mean error [mm]	std [mm]	Scanner resolution [mm]
Longuetaud et al. [25]	0.67	3.28*	0.36-0.81 x 0.36-0.81 x 1.25
Longuetaud et al. [27]	0.0	0.9	0.74 x 0.74 x 3.75
Cool et al. [29]	−3.0	7.2	1.43 x 1.43 x 4.0
Friedriksson et al. [31]	−1.87	4.87	0.605 x 0.695 x 1.0
Oja 1997 [24]	2.6	2.2	n.a x n.a x n.a
Andreu and Rinnhofer [26]	0.7	10.1	1.55 x 1.55 x 20
Breinig et al. [28]	1.7	4.0*	1.0 x 1.0 x 1.1
Johansson et al. [30]	−0.93	4.6	n.a x n.a x 10
Oja 2000 [32]	−2.0	3.0	n.a x n.a x 10

Table 2.3: Comparison between performances on knot diameter estimation.

Letting alone the one from Cool et al., obtained by working on images coming from a coarser resolution scanner with respect to the others adopting the same procedure in ground truth creation, and therefore not easily comparable with them, results in the first part of the table are generally better than the rest. This is most likely the effect of the CT-originated ground truth, which inherently guarantees higher performances with respect to measurements on wood, since excluding differences between actual defects and their scanned version.
In any case the performances on diameter available in the literature are already quite satisfactory, even if improvable still, while just a few, limited studies have been conducted on DKB, therefore leading to the need of new and more performing techniques.

Chapter 3

Materials and Methods

3.1 CT Log by Microtec

Since all algorithms and techniques described in the following of this work are developed and tested on data coming from the CT Log, the industrial log scanner by Microtec reported in Figure 3.1, the following section is devoted to a brief description of the technical specifications of such scanner, of the techniques it employs for extracting useful information for sawing process optimization and of the outputs it provides, alongside with some comments on the performances it achieves in terms of diameter and DKB coordinate estimation.

Figure 3.1: The CT Log [5].

3.1.1 Scanners in the wood industry

As the studies reported in the previous chapter suggest, since the middle Eighties the possibility of applying computerized tomographies to the detection and measurement of wood defects before sawing has appealed to more and more researchers and wood industry operators.

Anyway, the currently available literature mainly focuses on the feasibility of CT application to log scanning or on the performances of algorithm on tomographic data: a point that is not sufficiently stressed in most publications is the fact that, in order to be actually applicable in real case scenarios, all of these techniques and methods must be efficient and computationally fast enough to be run in the brief time span in which a log stays in the line before the actual sawing happens.
CT scanners designed to work in sectors other than the sawmill industry, given the quite different nature of their employment, are generally much slower than what is required in the sawing line, that is from 1 up to 4 m/s. In 2011 (the year in which Giudiceandrea et al. published the first work on the CT Log), the fastest medical scanner by Siemens (Siemens 2008), operated at at 0.5 m/s, while the average airport scanner for luggage had a speed of 0.3 m/s [4]. Furthermore, medical scanners necessitate of some time to cool down x-ray tubes between subsequent scans, thus making them even more unfit to the use in lines which typically operate continuously on all 24 hours.
These factors, alongside the need for real-time outputs and data processing, lead to the impossibility of application, even with specific adaptations, of such scanners to the sawing line, thus paving the way to ad-hoc scanning solutions. It is also worth pointing out that such solutions have not to bear the same degree of scanning accuracy as medical scanners, but can be perfectly suited to the task with coarser resolutions, especially along the longitudinal direction of logs, being the attention focused on general properties of wood defects, such as shape and maximum width in the case of knots, and not on the minute details of, for instance, the human body object of medical scanning. Such a "compromise" between speed and accuracy is exploited by CT Log, whose main features are reported in the following subsection.

3.1.2 Working principles and main features

In order to speed up its acquisition times, CT Log deviates from the typical configuration of tomographic scanner in terms of sensor disposition.
In brief, while the usual scheme employed in scanner is the so called *fan beam*, requiring several x-ray emitters and a matching number of linear sensors for data acquisition, each of which acquiring information about a limited portion of the scanned object, along the perpendicular line joining it with the emitter, CT Log instead employs the *cone beam* scheme, with only one x-ry emitter, but a wider, bi-dimensional array of sensors on the acquisition side [4].
A representation of the two different schemes is reported in Figure 3.2.
Given the different nature of its configuration, *cone beam* approach needs more advanced algorithms to yield satisfactory results, many of which come with computational complexities that make them unfit for use in real-time scenarios.
CT Log exploits an algorithm that was relatively recent and not implemented in other scanners at the time of its development, that is the one from Katsevich [33] [34]. This algorithm allows the scanner to perform a fast enough acquisition, still obtaining a fairly good output, thus making it fit to be used in the sawing line.
By means of employing this different beam geometry and by adjusting some other physical parameters (e.g. emitted power and gantry speed; further details, which can be found in the original paper and in [5], go beyond the scope of this work), the CT Log is able to guarantee the desired performances for its employment as an industrial in-line scanner:

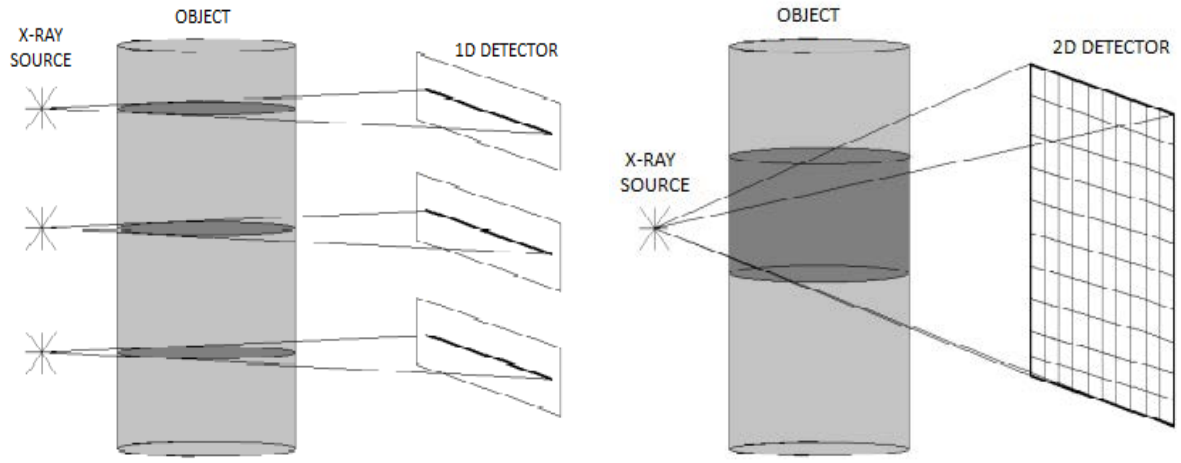

(a) Fan beam geometry.

(b) Cone beam geometry.

Figure 3.2: Different acquisition geometries for tomography [4].

- Scanning speed: 60 up to 160 $m/$minute, i.e. 1 to 2.7 m/s.
- Continued operating time: 24h per day, 7 days per week.
- Maximum diameter of scanned logs: 70cm, approximately depending on their density.
- Resolution of 1mm x 1mm for each bi-dimensional, transversal slice and of 10mm along the longitudinal direction of the log.

For more accurate specifications regarding what has just been reported and what will be mentioned in the remainder of this paragraph, [5] is to be consulted. Since up to 10 logs per minute pass through the scanner, CT Log is accompanied by an array of more than 10 computers, equipped with well performing GPUs, in order to perform image processing and log analysis tasks in a correspondingly short amount of time, i.e. well under six seconds, since in this time span the tomography itself has to be performed, too.
Taking as an example a six meters long log, all the processing steps required to gather the necessary information to sawing optimization would take about 25 seconds on a single, GPU-equipped computer: splitting the work among 10 of them, some of which performing specific defect-detection tasks, brings the overall processing time to approximately 2.3 seconds.
After the log has been scanned and the resulting information has been processed, an optimization software elaborates different possible cutting patterns, according to the specific kinds of product and product qualities required by the owner. This process involves the creation of the so called *virtual boards*, that is to say three-dimensional representations of the would-be final sawn products, each of which bearing information about the defects it would have after the cut. Having this information allows the software to estimate the product quality for every board and the whole log, and then to include this parameter in the final choice of the best cutting solution available for the specific log at hand. In one second, about 10000 virtual boards are created and analyzed to extract the optimal solution.
Figure 3.3 reports an instance of log split into virtual boards, each one with marks of different color identifying its main defects and features.

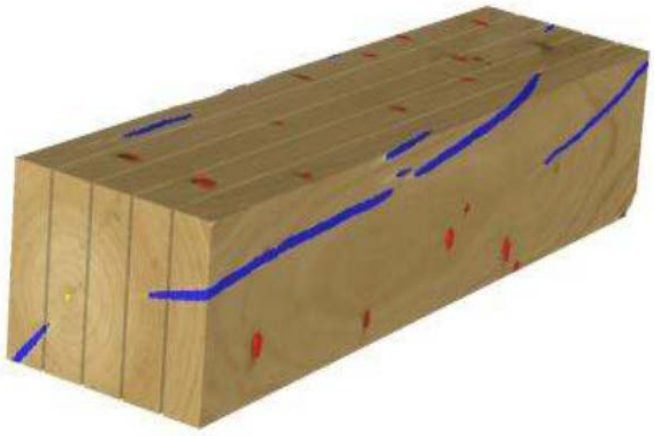

Figure 3.3: A representation of the virtual boards created by CT Log [5].

The choice of the best cutting pattern, which has to consider possible log rotations and different allocations of the boards in the log both in terms of positioning and of length, width and thickness, is eventually performed on the basis of some national or international grading standards, which most often take into account knots as the prominent defect afflicting product quality. A study regarding the ability of to achieve accurate grading according to one of these standards (more specifically the DAB one, mainly adopted in Germany) and to quantify in economical terms the benefit of applying CT image analysis before sawing is performed in [35]. This study, conducted on 36 Douglas Fir logs from which 172 boards were extracted, considers different product qualities defined by the aforementioned standard and different selling prices,and yields results showing that not only actual product grading was fairly accurately predicted by the machine, but also that the value of sawn boards with respect to a cut without a prior CT scan and the consequent optimization can increase between 4 % and 20 %. This fact, besides providing further proof to the goodness of the CT approach to sawing optimization, shows that CT Log is an effective mean to detect position and size of the principal wood defects, such as knots.

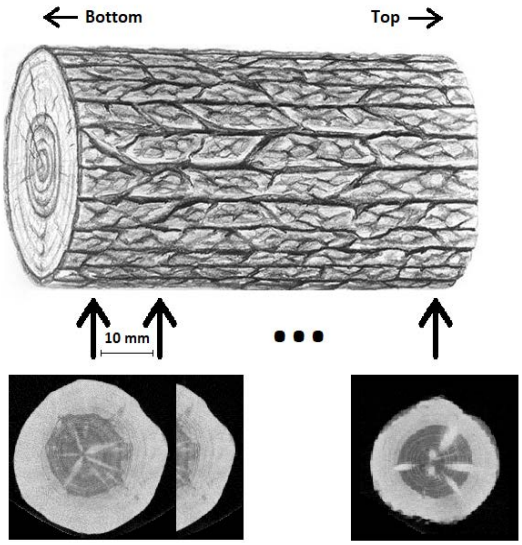

Figure 3.4: Representation of a scanned log.

3.1.3 Scanning a log: CT output and image processing

Original tomography and first processing steps

Before proceeding with the description of the procedures and materials used for the main goal of this work, it is necessary to continue with the description of the kind of images and log information provided by CT Log, which is also the starting point of what reported in the following: the two subsequent paragraphs, both containing material from [36] and [5] and images taken from CT Log, will be devoted to this purpose.
As previously mentioned, CT Log has a resolution of 1mm x 1mm x 10mm, meaning that each log is eventually scanned at one-centimeter intervals along its longitudinal axis, obtaining, for every interval, a slice with a 1mm/pixel resolution. Since the same amount of power is used for logs with different width, resulting images are sharper in correspondence of thinner trunks or even between different portions of the same log, being the base usually quite wider than the top for the phenomenon of secondary growth. This is a point to be taken into account since it can sometimes partially affect the performances of some algorithm. Figure 3.4 provides a representation of a whole CT scan of a log and Figure 3.5 shows how, in logs of different width, the quality of tomographic images tends to be different, too.

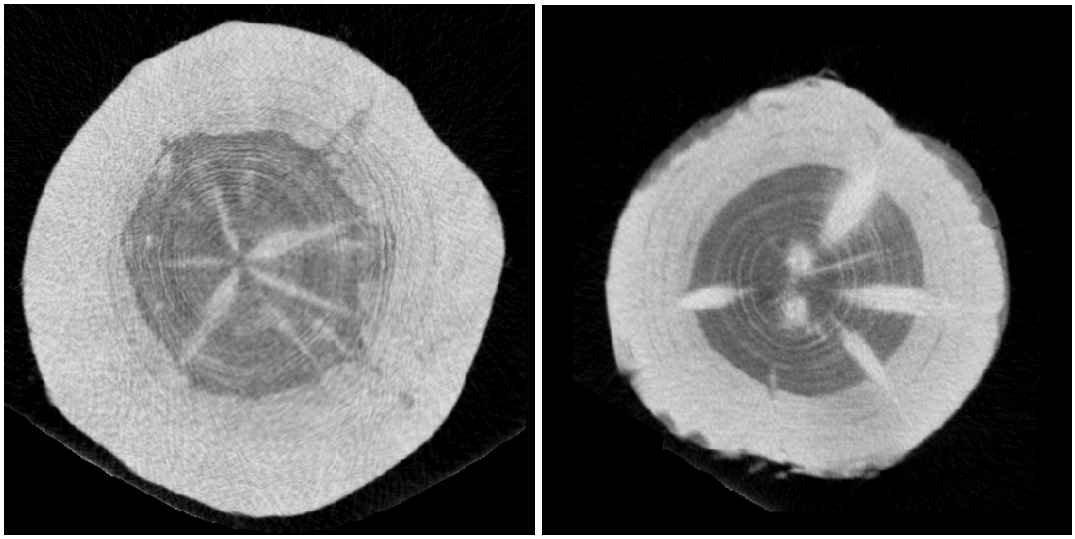

(a) Lower quality slice. **(b)** Higher quality slice.

Figure 3.5: Two slices from CT Log.

The two reported slices come from the very same log: it is anyway possible to notice how the one on the left, coming from the base of the trunk, carries more blurry details with respect to the one on the right, placed in the proximity of the top. The difference is more clear if focusing on growth rings,on the outlines of knots and on the less marked distinction between different elements in the image (e.g. heartwood-sapwood).
This image set provided after the tomographic scan of the log is then processed via some computer vision algorithms of different complexity. Some minor features and defects are identified, such as the presence of bark, rot, metal inclusions in the wood, the width of growth rings, resin pockets and heartwood-sapwood border: these are the minor operations, requiring simpler procedures and fewer computational power.
Some major tasks, or at least more important since affecting other subsequent steps, are also

performed: the first of them is pith detection, which plays a crucial role since providing the starting point for most of the knots and because many defects and features are placed in a radial fashion with respect to it. Being the center of year rings, the pith can be identified by mean of the Hough circle transform applied on each slice. Inter-slice continuity in pith position has to be guaranteed by means of some regularization filters, since the position of the pith in the slice plane at different transversal coordinates, if plotted in two dimensions, biologically follows a regular curve (except in the case of severe wood defects suck as cracks or broken tree top).
Once these steps are performed, log processing continues with knot detection and parameter estimation.

Knot detection, extraction and analysis

Before proceeding, it is necessary to make some clarity on the way different coordinates are referred to in the following: when dealing with the tomographic images coming from CT Log, horizontal and vertical image coordinates in the transversal slices of the log will be addressed as x and y respectively, while the longitudinal coordinate (i.e. the one varying slice by slice) is defined as z. It is also worth pointing out that the z direction is not necessarily the one coinciding with the one in which the tree grows, since a log can be scanned either starting from its top or its bottom indifferently.
When dealing with knots, instead, since they will be extracted in separated voxel blocks (as described in the following), coordinate naming will be slightly different: as already mentioned in Chapter 2, the vertical coordinate in slices belonging to knot blocks, corresponding with the one parallel to log radius and therefore defined as *radial*, will be marked with r, while the horizontal one will be labeled as t (transversal). The coordinate ranging in knot slices will be referred to as l (longitudinal), and it can, once again, coincide both with knot vertical growth direction or with its opposite, according to how the entire log has been scanned.
Knot detection and parameter estimation is performed in three main phases, hereafter listed and subsequently described:

- Slice segmentation via a CNN.
- Knot detection (also known as identification): definition of knot bounding box and knot block extraction.
- Knot area analysis, comprising knot parameter estimation.

For their extraction in separate voxel blocks, knots are to be, as a first thing, isolated from the rest of the image: this is performed by a segmentation operated via a CNN on each slice provided by CT Log.
The CNN takes as input a voxel block composed of 5 stacked slices, each of which is reduced to the dimension of 128 pixels both in the x and y axis to keep consistency across logs of different sizes. Its output is an equally-sized voxel block, having values in $[0,1]$, each of which expresses the probability that each voxel belongs to a knot. In the subsequent Figure 3.6, the image on the right reports one of the five slices composing an input block, while the right is the corresponding output provided by the network.
The dataset used for training such CNN was constructed by manually marking the slices resulting from the scan of 75 Scots Pine logs coming from all over Europe, resulting in a total of over 10000 knots. The marking proceeded as follows: exploiting a dedicated software from

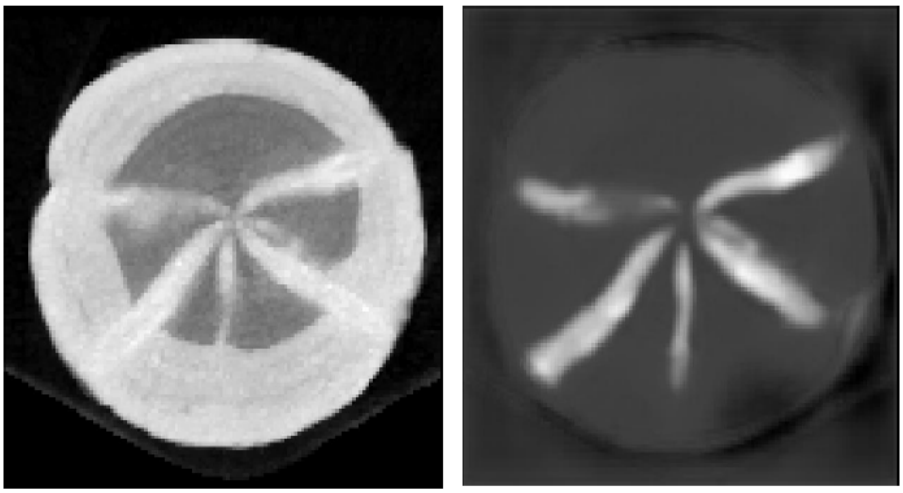

Figure 3.6: Input and output of the CNN employed in slice segmentation [5].

Microtec, each knot of each slice was isolated by hand-picking its starting and end points, its diameter at different positions in r and its DKB (again, marked as the coordinate of the maximum diameter). Moreover, any number of additional points could be added to each knot to better define its shape, since many of them can exhibit irregular curvatures depending on the condition under which their growth happened.
To provide a better understanding of how this software works, and also because of its further use importance in the creation of other datasets employed in the following, a screenshot of it is reported in Figure 3.7.

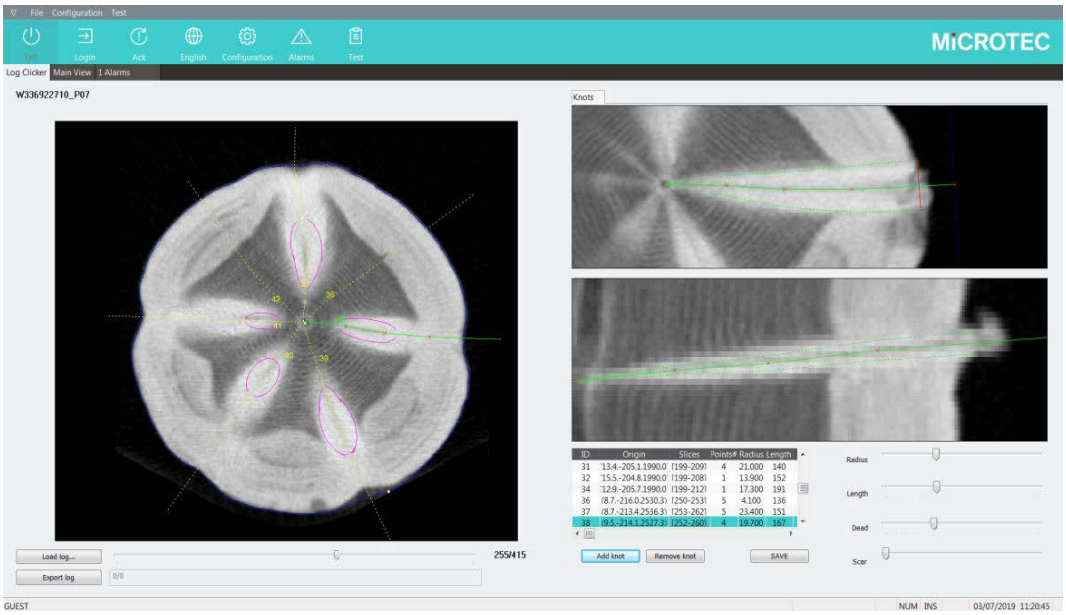

Figure 3.7: The software employed in knot labeling [5].

As it is clearly visible in the top-right slot, 5 points are marked in a single knot (corresponding to the one whose axis is green on the whole slice on the left), thus allowing to sharply define its outline. DKB, and therefore knot diameter, is marked as a red line perpendicular to the axis marking radial direction.
The information obtained by means of this software was then adapted to the aforementioned

slice blocks to serve as ground truth for network training by marking with one each voxel belonging to a knot, according to its hand-defined version, and to 0 each voxel not belonging to any.
In order to get voxel blocks of fixed size for each knot, the information coming from slice segmentation has to be exploited to locate every knot in the three-dimensional tomography and to define a bounding box around it, so to gather the necessary parameters to fit it into a block. Under the simplifying assumption that, for every knot, its axis can be modeled as a straight line starting from the pith, providing that pith position is known at each slice (as it actually is, as previously described), only three parameters are needed for its description: its starting point along the z axis and two angles, that is the one relative to the direction of knot axis projection on the x-y slice plane and the one formed by the axis and the slice plane itself. Given a range of slope values in which the actual two just mentioned angles are reasonably expected to fall, that is, specifically, $[-30\%, 30\%]$ with a 2% step, it is possible to define one and only one axis per voxel (in the whole tomography) connecting it to the pith. This step allows to define an angle between knot axis and slice plane and to obtain a precise pith coordinate, i.e. the one intersected by the axis itself; the angle formed by knot projection onto the x-y plane can be calculated by means of a plain $atan2(\cdot)$ operation, since x and y coordinates of pith and considered voxel are known.
Given this triplet of parameters, a three-dimensional line, modeling knot axis, can be defined. Actual knots positions are then estimated by applying a 3D Hough map to these lines and by exploiting the information coming from the previous step to calculate the probability that a triplet of parameters actually belongs to a knot. Local maxima resulting from this process are selected as correct values for the determination of knot axes.
Once its position is available, a block of voxels containing each knot bounding box is extracted. Blocks employed in the course of this work have a fixed size of 128 x 64 x 12 along the r, t and l directions, respectively: since not all knots may fit into this block size, (possibly different) scaling factors are sometimes applied to the knot representation along one or more of its three direction. This information has to be carried along with the block for all the processing steps it goes through, since any parameter estimation performed on it has to be the re-scaled according to these parameters. Such scaling factors are applied a-priori of every processing steps according to some heuristics concerning log radius and maximum expected knot diameter.
An instance of knot block, in which the l coordinate progresses from left to right (i.e. all the 12 vertical slices have been aligned) is reported in Figure 3.8. When referring to this kind of images, in the following, the t coordinate will span from left to right starting from the top-left corner of each image, while the r one will span from top to bottom starting from the same position.

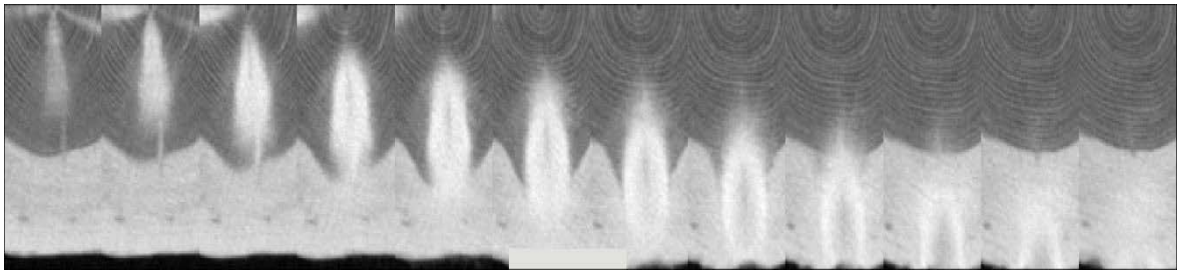

Figure 3.8: A knot block [36].

As it can be seen, image by image, the approximately elliptical shape of the knot can be found at increasing *r* coordinate: this happens because the *r-t* plane intersects the knot at increasing *l* coordinates (each spaced of 1*cm* because of the resolution of CT Log), thus including a higher and closer-to-log-edge portion of knot, as it can be inferred from Figure 2.7 by imagining each slice as a plane cutting perpendicularly to the Figure itself and in parallel to the bottom. At this point, the process followed by the software accompanying CT Log differs, for what concerns diameter and DKB coordinate estimation from the one proposed in the following of this work: a CNN for semantic segmentation is again applied to the just extracted knot blocks, its output being very similar to the one described in the first part of this paragraph (it is reported in Figure 3.9a).

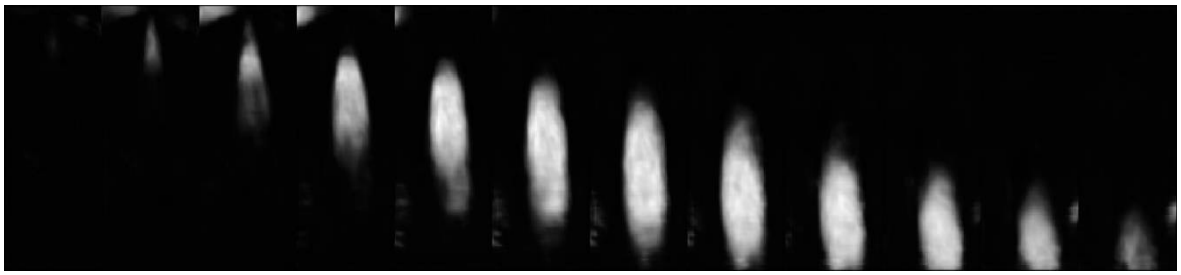

(a) Knot block processed by the CNN for segmentation [36].

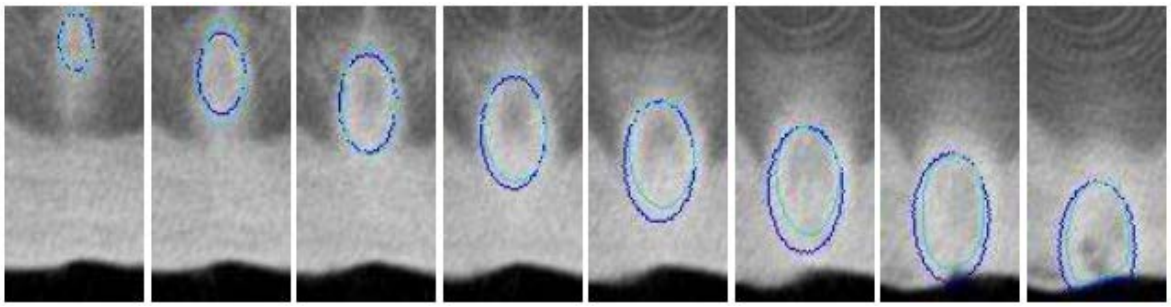

(b) Output (light blue) and ground truth (blue) for segmentation [5].

Figure 3.9: CNN for knot segmentation.

Once the CNN output is available, knot parameters are straightforwardly measured, including knot length, end point, diameter and DKB *r* coordinate (in correspondence of diameter).
For the training of the network more than 5000 blocks were manually labeled by means of a dedicated software. Figure 3.9b reports the superimposition of marked ground truth and CNN output for an instance of knot used in the development of such network. CNN prediction is represented by the oval in the darker-blue color, while the corresponding ground truth is signaled by the lighter one.
The whole process allows to correctly identify the vast majority of knots, for most species even in sapwood, and to extract the corresponding blocks, with only a small fraction of imprecise detection mainly due to the presence of defects exhibiting a quite similar aspect to knots when scanned, such as pitch pockets, or to the presence of knots growing in very tight clusters, thus allowing to extract several tens of instances from each log. Other defects or log features such as rot or dried wood do not affect this step, but have a partially detrimental effects in the procedures described in the following.
Knot parameter estimation, though, is more prone to small errors, mainly because of some imprecision introduced by CNN output, in the case of diameter, or because modeling the

DKB coordinate as exactly the point in which diameter stops growing may not always be very accurate, since the portion of sound wood in the knot can, in some cases, continue quite beyond that point.
No accurate estimation of the performances of these algorithms were currently available before the development of this thesis, mainly because of the difficulty (dealt with in the remainder of this work) of obtaining a proper physical ground truth for DKB and diameter values. Anyway, empirical observations on final sawn product suggested that the estimation of these two important parameters leaves some room for improvement.

3.2 Designed procedures and employed datasets

In order to improve performances of knot parameter estimation, four different approaches involving CNNs are tested. Each of them differs from the others either in the followed procedure or in the construction of the dataset employed in network training.
While the first approach consists in the basic application of a CNN to each knot voxel block to perform direct regression of parameters, the second tries to extend knot analysis by first determining knot status, in order to cope with the presence of fully sound knots not having a DKB coordinate. The last two procedures, only differing in dataset construction, aim to design a more computationally efficient and accurate strategy tackling both the issues of status determination and, in case of knots deemed as dead, of DKB coordinate and diameter regression, at once.
Each approach employs a different dataset according to the specific problem at stake: in the first two cases, CNNs are trained on ground truths obtained by inspection of CT images, the first of which was already available since employed for other research purposes, while the second was gathered in order to obtain more sound knot samples. The last two datasets differ from previous ones since designed to rely on manual measurements, and therefore no software defined diameter or DKB position is available in this case; they only differ in block extraction, as explained in the description of the last approach.

3.2.1 Approach 1: direct regression of DKB coordinate and diameter (DR)

Procedure

The first and most straightforward approach to the problem of diameter and DKB coordinate estimation consists in performing their direct regression (from here the abbreviation DR, with which this procedure will be mentioned in the following) by training a simple network aimed at receiving the whole voxel block containing a knot as input and providing the parameter as output. Two different approaches, respectively referred to as DR1 and DR2, involving the training of three separate networks are followed:

- DR1.Training and testing of two CNNs, one aimed to perform diameter regression and the other with the goal of regressing DKB coordinate.
- DR2. Development of a single convolutional network performing the regression of both parameters at once. This approach aims at exploiting the inherent correlation between the two quantities of interest, since DKB coordinate is most often in the close proximity of the maximum diameter.

Given the similarity of the faced problems, all three networks are envisaged to have a similar structure, too.
To be ideally placed after knot block extraction in the course of log analysis, the main goal of these CNNs is to serve as preliminary test for designing suitable network architectures for the problem at stake since, as explained in the next paragraph, the structure of dataset employed in network training has a considerable impact on obtained performances and on their overall reliability, especially in the case of DKB coordinate estimation.

Dataset

The voxel blocks used in this stage, even though extracted by the same procedure described above and also employed in the following, were originally obtained for other testing purposes (out of the scope of this work) and therefore are slightly different in their dimension, presenting in fact only 8 l slices instead of 12. The difference is, anyway, not very marked since most knots are contained in a span of 8 consecutive CT images and only a few exceed this size.
The dataset is then composed of 549 128 x 64 x 8 (t x r x l) voxel block coming from Scots Pine logs scanned with CT Log. Ground truth for diameter and DKB coordinate are obtained by the means of the same software employed in the marking of knot necessary for the CNNs mentioned in Section 3.1. One of such blocks is reported in Figure 3.10

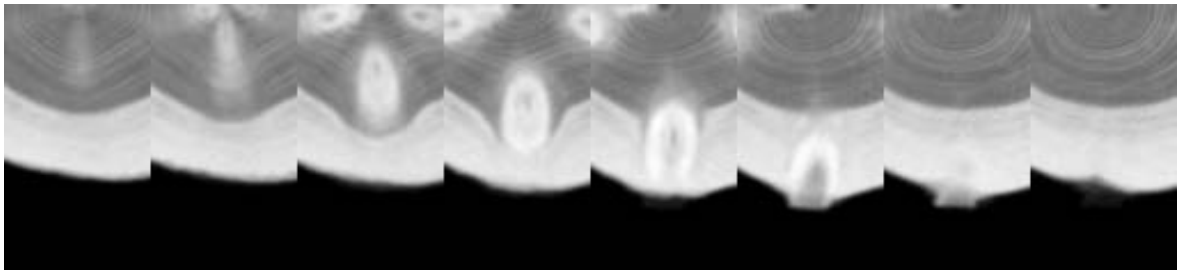

Figure 3.10: Knot block from the first dataset.

It is again worth pointing out that, while this procedure may be quite accurate in providing a ground truth in the case of diameter, its precision in DKB coordinate determination remains questionable. Moreover, the composition of this dataset appears to be slightly biased towards knots coming from relatively small logs and showing very few irregularities, meaning that the vast majority images are very sharp and well defined if compared with real-life scenarios.
Anyway, such dataset is still good to perform preliminary tests to explore the viability of the CNN approach in the field of knot parameter estimation.

3.2.2 Approach 2: determination of knot status and model fitting (SD)

Procedure

One of the major inconveniences in the procedure described in the previous paragraph is that it requires an implicit assumption: when determining a DKB coordinate the knot is implicitly supposed to be dead at some point. This does not always hold true, since in many cases, especially in the ones of bigger knots growing in proximity of the top of the log, no actual DKB coordinate can be found. It is indeed possible to set a default value of DKB to, for instance, the maximum r coordinate as ground truth for sound knots, or in any case to use

similar expedients, but the limited amount of available samples and some preliminary tests performed in this direction indicate that such an approach is not optimal, since several tested network configurations struggled to converge when trained with an adapted version of the dataset.
A new procedure, referred to as SD, for "Status Determination" is then to be designed in order to take into account the presence of a not negligible share of sound knots. A simple CNN for the task of binary classification is an effective means of distinction between wholly sound knots and knots dying at some point in the block: it has to be applied prior to the one performing parameter regression or even to the one providing diameter and DKB coordinate estimation via semantic segmentation, already working in in-line applications.

Dataset

Despite the apparently simpler procedure described in this second step, dataset creation proves here to be a little more delicate than in the previous case. This is mainly because, being the distinction between an overall sound and dead knot obviously more marked than the possible error made in the estimation of knot parameter, mislabeled samples has higher detrimental effects. Such classification besides presents the possibility of several uncertain cases in which the knot actually dies, but does so in close proximity of log edge, making thus the correct labeling highly uncertain, or in some cases not at all possible when starting from CT images only.
A reasonable solution would be to mark all such uncertain knots as either sound or dead, depending on which bias is less costly to introduce in the network: this is possible since the sound-dead transition would happen, in the vast majority of these cases, in an area of the log where valuable sawn products are very unlikely to be obtained, therefore limiting the detrimental effect of a misclassified knot in a board. It is anyway to be pointed out that, once again, the effect of introducing such a bias in the training of a CNN has difficultly predictable effects on the outcomes of its classification. Furthermore, in this specific case, very few samples are available: since the physical ground truth is not accessible, only few sound knot samples can be identified with reasonable certainty.
Employed criteria to mark a knot as sound are:

- As obvious pre-condition, the knot must reach log edge.
- Its diameter has to keep, even very slightly, growing for increasing r coordinates, or at least not staying constant for a significant portion of a slice. Notice that this is a slightly weaker condition than the one imposing DKB coordinate (and therefore the presence of a dead knot) in correspondence of coordinate where maximum diameter is reached.
- Sapwood border must bend outwards in the direction of log edge, creating a characteristic curvature around knot borders, which signifies that wood fibers are, in that area, still feeding a growing and thus sound knot.
- Knot borders in sapwood have not to be too sharply defined, since this again signals the presence of a significant portion of sound, growing wood.

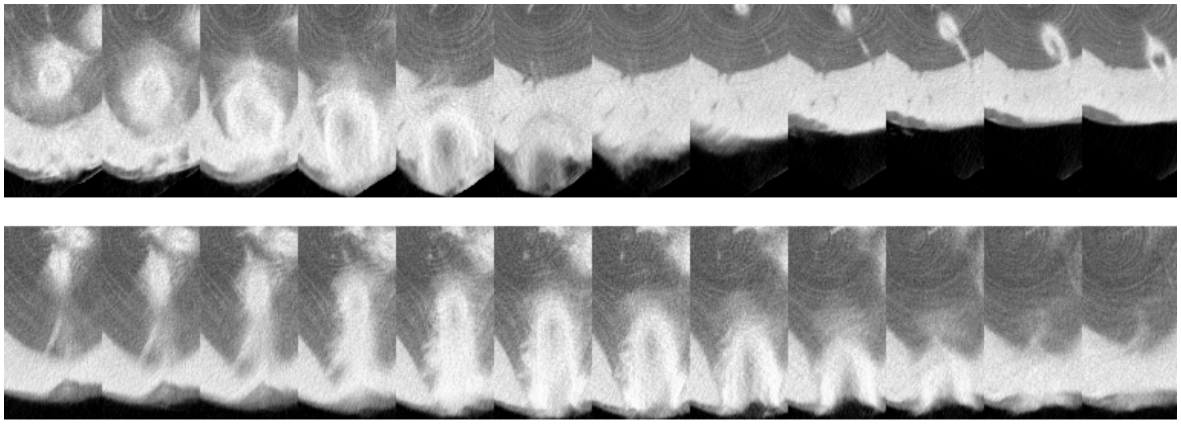

Figure 3.11: Two examples of sound knot.

Figure 3.11 reports a couple of knots marked as sound. It clearly visible how they both respect the previously defined criteria: sapwood bends in correspondence of the growing knot, their outlines are not too sharply defined against sapwood itself and their diameter keeps increasing up to log edge.
To a large majority of knots selected in this fashion, a group of others coming from actual observation and classification performed on real logs are added. Such knots all present the distinctive feature of reaching the exterior of the log, since originally collected for testing the performances of CT reconstruction and subsequent analysis on this specific kind of defect. They are, thus, bigger in size than the average knot, but provide the means of giving the network some information about the limit-cases in which a big knot reaching log edge is dead (most likely right before the edge). They are of particular importance since, if labeled by an observed just starting from CT images, correct classification could prove to be particularly difficult to achieve. An example of such dead knots is reported in the following Figure 3.12.

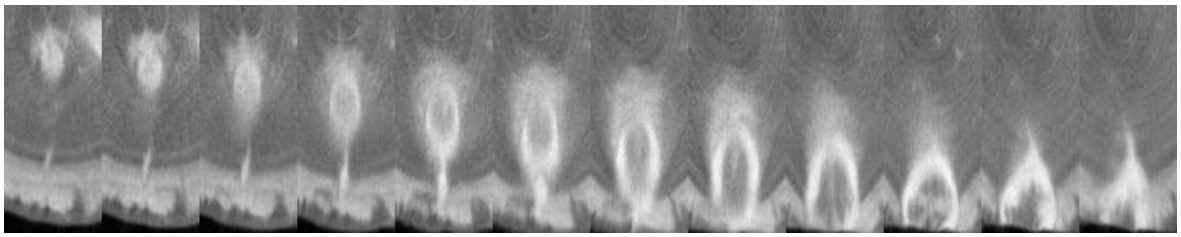

Figure 3.12: A dead knot reaching log edge.

It is clearly possible to see why such kind of knots can prove tricky to classify only starting from tomographic images: besides reaching log edge, this knot, which was classified as dead from the observation of its portion reaching the outside of the log, presents a quite marked bend in the sapwood area around it and seems to have a slightly increasing diameter for all the images (except, perhaps, two of the last three). Its outline appears, though, in quite sharp contrast with the surrounding sapwood, thus providing a clue of its real status.
Even though some of this valuable examples with a verified sound/dead label are available, many knots coming from CT scans present similar features, but lack for a certain ground truth: only a small portion of them, i.e. the ones for which labeling was assumed to be correct with

an high degree of certainty after the inspection of an expert forest scientist, are included in the final set of samples employed in network training.
The dataset results to be eventually constituted of 343 sound knots and an overall pool of some hundreds dead ones coming from several tens of Scots Pine logs. At the moment of CNN training only 343 dead knots are considered to guarantee a fair balancing between classes. Ground truth certainty coming from real-world observations is available for 30 sound knots and 35 dead knots. It is also worth mentioning that, in some cases in which labeling is deemed as too uncertain, a bias towards sound knots is adopted, given that, as previously explained, uncertainty in parts of the log closest to the edge does not have highly detrimental effects on final products.
An even smaller number of Maritime Pine samples are available, too (around 30 of them sound): given their relative similarity, when scanned, to the Scots Pine ones, they were also kept into consideration during network training and testing.
The reduced number of available samples, mostly due to the uncertainty of correctly labeling a knot reaching log edge, limits the scope of this approach since providing a restricted amount of information for proper network training. This procedure remains, anyway, a valid test for future developments of this approach to knot analysis since, as reported in Chapter 4, some preliminary simulations yield promising results.

3.2.3 Approach 3: estimation from sparse measurements and manually marked knot blocks (SMS)

The two previously described strategies, even if still promising under some aspects, bring to light some major issues that can be encountered when designing efficient way to perform real-time, in-line knot parameter estimation:

1. Difficulty in obtaining accurate measurements of diameter and DKB position.
2. Sound/dead knot labeling can prove quite imprecise in larger knots.
3. Determining knot status and estimating its parameters in a following steps is potentially a computationally-costly operation.
4. The lack of fairly accurate measurements and ground truth makes it hard to correctly evaluate performances.

For what regards point 1, obtaining a suitable amount of good-quality data to train a CNN for diameter and DKB coordinate regression is a rather lengthy and hard to achieve task, since it can either be performed by creating the ground truth via a software, thus leading to possible remarkable discrepancies with respect to the real values, or by manual measurements on physical wood samples, as performed by some authors whose works have been reported in Chapter 2, which is a time costly method only allowing to gather relatively small quantities of samples and is then more suited to studies concerning the feasibility of the CT approach or the development of algorithms not exploiting neural networks.
Point 2 was already explained in the previous subsection: performing binary classification on the whole knot can lead to uncertain outcomes.
The third point has not been yet mentioned, but can have significant outcomes in in-line applications where computational efficiency plays a major role. Moreover, introducing two separate steps can lead to more potential sources of error.

Eventually, point 4 is probably the most important: both the strategies designed above are either difficult to be measured in terms of performances and to be compared to each other: this is mostly due, again, to the difficulty in constructing accurate datasets.
It is therefore desirable to design a procedure capable of efficiently determining both knot status and parameters, possibly employing a large dataset, whose reliability has to be higher than the one provided by the manually-marked ground truth created via an ad-hoc software (it has therefore to come from physical measurements). A change of perspective is then necessary in terms of the way the CNN is applied to input blocks and of how performances are measured: a possible way of doing so is to exploit a dataset constructed as explained in the following. The description of the adopted procedure is here postponed since strongly dependent on dataset structure. This approach will be represented by the abbreviation SMS, standing for *Sparse Measurements, Software*. Software refers to the means of block extraction.

Dataset

The approaches followed up to here are strongly focused on the precise value quantities of interest have, in the sense that they aim to directly obtain its estimate, thus incurring in the ground truth related issues mentioned above. The ultimate goal of this work is, anyway, to define a performing procedure to estimate with reasonable accuracy knot parameters to improve the quality (and thus the selling price) of sawn products.
It appears therefore reasonable to shift the goal of designed networks and algorithms towards the analysis of data coming from actual boards and to try considering suited datasets for this purpose, since in this way no perfectly accurate DKB ground truth or overall knot status knowledge for each knot are needed in order to develop new approaches (it is only necessary to be able to predict whether a knot intersecting a certain board is either dead or sound at that point), with the additional benefit of being able to obtain more accurate performance measurements for the designed procedures since having a perfectly observable ground truth at disposition.
It is under these motivations that a completely different paradigm is envisaged in this paragraph: the employed dataset consists of a set of a variable number of *samples* per knot, obtained by measuring knot diameter and status of each knot on sawn boards and associating such values to the corresponding r value on each block of CT slices containing the very same knot measured on physical boards.
In other words, a similar procedure to the one described in [35] or, equivalently, in [37], was followed with the replacement of knot blocks instead of reconstructed boards: 15 Scots Pine logs (only 13 of which were actually employed in dataset creation) were marked by drilling two holes on their bottom to serve as reference point for the following steps, one in correspondence of the pith and the other in proximity of log edge. Another reference hole was drilled on log top. The logs were then cut in thin boards 15 millimeters thick following a regular cutting pattern; after cut the position of sawn boards with respect to the reference holes was noted in order to allow for the reconstruction of their exact position in the original log once removed for performing the necessary measurements.
Figure 3.13a reports the bottom of a log with the reference holes already drilled: they are the topmost and lowermost ones, the other dots being only additional auxiliary points performed with a permanent marker. Figure 3.13b gives a hint of how the cutting pattern was designed: it is worth noticing that boards were fit to span the whole log, even in close-to-the-edge zones from which valuable products are hardly ever extracted. Board edges were not refined in order to keep as much information as possible.

(a) Bottom of the log with reference holes. **(b)** Log cut into thin boards.

Figure 3.13: Two slices from CT Log.

Every knot on each board was then inspected by an expert who noted its position on the board, its status and diameter. Three different knot statuses were taken into account: sound, dead and transitioning (i.e. only partially surrounded by bark or uncertain): this latter category will in the following be treated as belonging to the "dead" samples, since such knots exhibit closer properties to black knots than to sound ones.
The final step in ground truth creation required some adaptations to the software employed in the previous subsection and reported in Figure 3.7 in order to combine the information coming from manual measurements and the actual position of knots in the log.
As a first thing, the chosen cutting pattern had to be reconstructed in the software by aligning the position of actual boards (to be rendered in their digital counterpart, the *virtual boards*) to the reference holes, so that to also align each knot with its original position in the log. A representation of this process is reported, for clarity, in Figure 3.14.

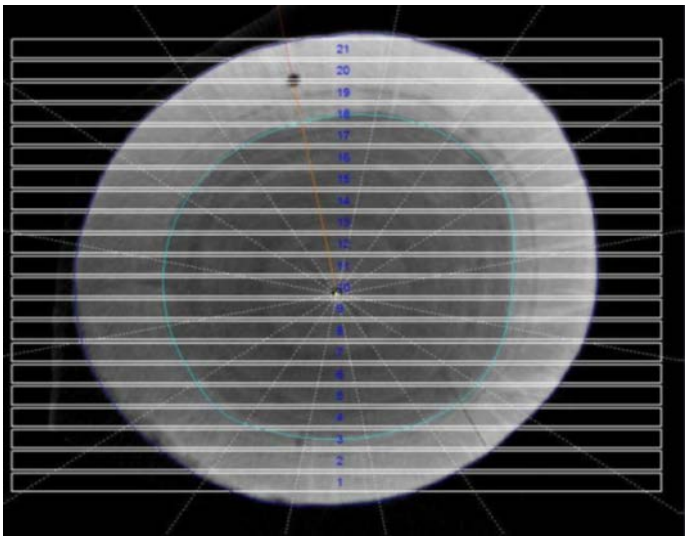

Figure 3.14: Aligning virtual boards to the reference holes.

Each knot containing one or more measurements was then inspected via the software and its origin and end points marked down. After making sure the alignment of virtual boards with real ones had achieved sufficient precision, the r coordinate of each knot sample on every board was computed by firstly intersecting knot axis with the corresponding virtual board and secondly by projecting, in the board plane, the hand measurement onto the knot axis. This point is further clarified by Figure 3.15.

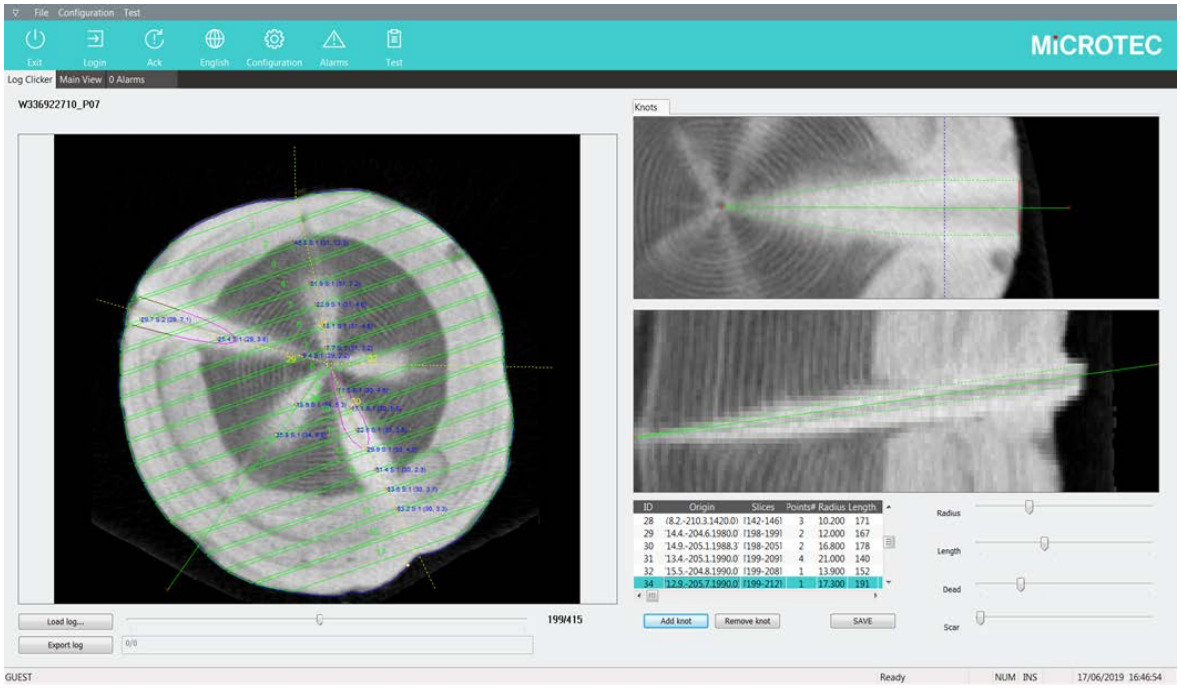

Figure 3.15: The modified labeling software.

Considering the log displayed on the left, hand-marked knot profiles with the corresponding axes drawn in yellow are present as in the original version. The reconstructed cutting pattern is visible as a series of (in this specific case) 17 progressively numbered virtual boards represented in green. Each measurement performed on real boards (also referred to as "sample") is reported in blue.
Inspecting the Figure, it is possible to better understand how the determination of the r coordinate for each sample works: considering the topmost, central sample, for instance, it is first necessary to determine at which point knot axis intersect virtual board number 2, and then to associate the measurement to such intersection, having slightly mismatching coordinates in the board plane and also being different from the plain distance from knot axis.
When the pairing between real knots and their scanned counterparts was completed, a list of samples with the relative status, diameter and r coordinate was available for each knot: excluding the cases of misaligned measurements (e.g. their position on virtual boards was more than 1cm apart from the closes knot axis) a knot block was extracted for every knot to serve as input for the CNN described in the next paragraph.
An instance is reported in Figure 3.16.
It is important to point out that such blocks differ from the ones provided by the software accompanying CT Log since they are extracted starting from manual measurements on the scanned log and centered (along the t axis) on a precisely defined knot starting point, while

automatically extracted blocks may present some (even relevant) misalignment, especially in the case of irregularly shaped knots presenting some curves along their axis.

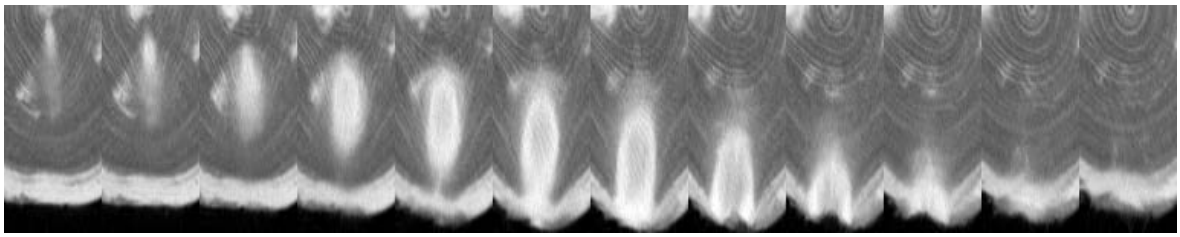

Figure 3.16: A block extracted by the modified version of the labeling software.

In total, 634 valid voxel blocks were extracted out of the 13 logs, each of which was relative to one or more of 2412 knot measurements performed on real boards. Each knot block is associated with possibly several samples both belonging to the sound and dead classes (up to 6 or 7 in total, in the case of large knots):

Procedure

Such dataset structure requires a novel approach with respect to the ones previously described and to the ones available in the literature. A new performance metric is needed as well, since having only some sparse samples for each knot and therefore the lack for a well defined ground truth reference measurement does not obviously allow for the determination of a mean error and its standard deviation. For this reasons, the focus is here shifted to the accuracy, in percentage, with which designed algorithms can predict the status of a knot on a given board. The input to the CNN is also reconsidered: instead of acting on the whole knot, the network is now designed to operate on small sub-portions of the block. More precisely, if the original dimension was 128 x 64 x 12, now the input has now size 15 x 64 x 12, while the output still remains a binary classification indicating whether the knot portion is, as a whole, either sound or black (for the moment the focus is posed to the problem of knot status determination, while diameter is left for a latter stage).

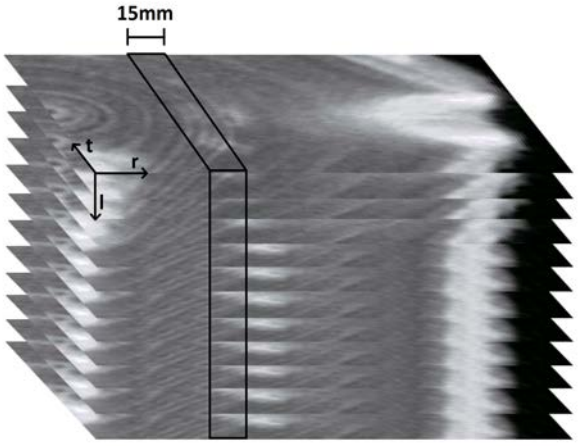

Figure 3.17: A knot block with an highlighted sub-portion.

An intuitive representation of such sub-portions is provided in Figure 3.17: representing the knot as a block of stacked slices, the input fed to the network is a part of it covering the whole t and l dimensions, but only spanning 15 pixels in the r one.
For biological reason, if a knot is sound at a certain r coordinate it must be so also in all the preceding ones and, on the opposite, if it is dead for some r all subsequent samples for increasing coordinates are black, too. It is thus possible to extract, from every knot, much more sub-portions with a valid sound/dead label than the number of available samples coming from measured knots on boards.
In this way, if extracting a 15 pixel wide sub-portion centered around each pixel for which certain sound or dead label is made available by the presence of a subsequent or preceding measured sample respectively, technically only two samples per knot, if available, are truly needed in order to get a quite large number of sub-blocks for network training: the sound sample having maximal r coordinate and the dead sample having the minimal one. Observing Figure 3.18, such samples are marked as *Ms* and *md*.

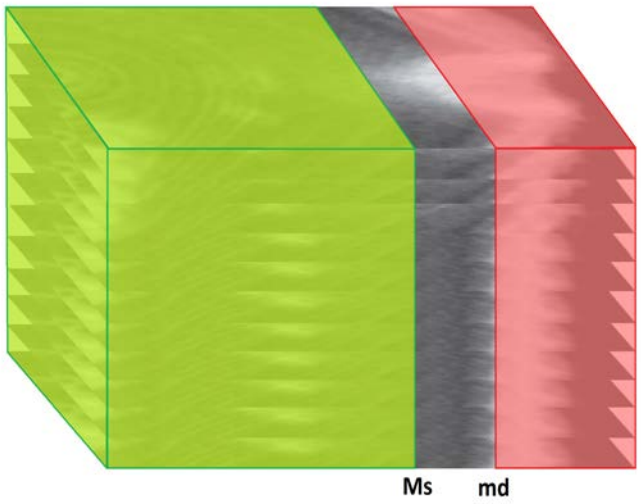

Figure 3.18: Zones with certain labeling provided by *Ms* and *md*.

The area colored in green contains all the pixels which provide reliable "sound" labels for knot sub-portions centered around them, while the one in read signifies the same for sub-blocks to be labeled as dead. The area left in gray is the one for which no information is available, due to the nature of the employed dataset.
Once a sufficient number of training sub-blocks for the network is extracted and the CNN effectively trained, a status predictor for dead knot sub-portions (marked here on with label 1, while sound ones are labeled as 0) is available and ready to be applied in the second part of the process, that is the one actually concerning knot status prediction on single boards.
Even though this paragraph started with the consideration that a proper ground truth for DKB is not available, the estimation of such coordinate could still be useful as a mean of predicting knot status on virtual boards before cut: it is of course possible to apply the CNN for classification on sub-portions centered around the coordinate intersecting each board, but this process would be indeed computationally expensive, if considering that several thousands cutting pattern simulations are performed before the best one is actually chosen, thus leading to the need to apply the CNN on nearly every one of the r pixels.
So the best solution remains to exploit the structure of the network, together with the same

biological notions employed for labeling sub-portions, to create an algorithm capable of providing an estimate of DKB position and to then determine knot status at each r coordinate by comparing it to the obtained estimate.
To perform this task it is not necessary to obtain a prediction for blocks centered around each of the 128 r pixels: in order to achieve higher computational efficiency and thus make the process more suited to run on in-line applications it suffices to identify the region where network output consistently transitions from 0 to 1, signifying that DKB has been surpassed. once this zone has been spotted, a pixel-wise analysis can be performed (with the same selection criterion) to determine the final DKB coordinate. An example is reported in the following to better clarify this point.
Consider, for instance, an ideal case in which the CNN always correctly predicts sub-portion status and the DKB is placed at the $101th$ pixel, numbered as 100 since pixel count starts from 0. By applying the network to each pixel, the result is a vector of outputs of the kind:

$$0\,0 \quad \cdots \quad 0\,0\,0\,1\,1\,1 \quad \cdots \quad 1\,1,$$

where the first one corresponds to pixel 100. The result does not change if only considering non-overlapping sub-blocks, i.e. applying the classification to blocks centered every 14 pixels (sub-block dimension minus one), starting from the first available one, in this case the eight pixel, numbered as 7. In this way, a vector of only 15 values is obtained, including predictions for sub-blocks centered around pixels 7, 21, 35, 49, 63, 77, 91, 105, 119, resulting in the following vector:

$$0\,0\,0\,0\,0\,0\,0\,1\,1,$$

with the last 0 being the output of the network applied to the block centered around 91 and the first 1 corresponding to pixel 105.
By iterating the same procedure, this time pixel by pixel, between these two points (not included) we get the output:

$$0\,0\,0\,0\,0\,0\,0\,0\,1\,1\,1\,1\,1,$$

with the transition happening, once again, at pixel 100.
Thanks to this simple expedient, only a reduced number of positions had to be checked in order to provide an estimate of DKB position. Anyway, when working under the more realistic assumption of imperfect CNN outputs, some small modifications have to be taken into account.
A way of compensating for errors introduced by wrong predictions is to select as transition point the one in which such transition becomes fairly stable, that is the one in which the number of 1s on the left equals the number of 0s on the right, assuming the network misclassifies a sound sub-block as dead and vice-versa with equal probability.
While it is easy to see how the previous case is correctly managed by this procedure, another example is here after reported in order to make further clarity. Let us assume that the output vector (128 pixel considered) takes the following forms:

$$\begin{array}{lllllllllll}
0\,0 & \cdots & 0\,1\,0 & \cdots & 0\,0\,0\,1\,1\,1 & \cdots & 1\,1\,1 & \cdots & 1\,1, \\
0\,0 & \cdots & 0\,0\,0 & \cdots & 0\,0\,0\,1\,1\,1 & \cdots & 1\,0\,1 & \cdots & 1\,1, \\
0\,0 & \cdots & 0\,0\,0 & \cdots & 0\,0\,1\,0\,1\,1 & \cdots & 1\,1\,1 & \cdots & 1\,1.
\end{array}$$

In the first case, the CNN mistakenly classifies as dead a slice in the first part of the block: the selected DKB coordinate is, in this case, the one marked by the last 0, since the number of 0s

on its right (including itself) is equal to the number of ones on the left. The second case is perfectly analogous, but with the opposite classification error.
The last vector reports the case in which both errors are present in equal number (represented as a simple 0-1 swap in proximity of the DKB for ease of visualization). In this case, the selected DKB coordinate is the correct one, since the effects of the two errors cancel out.
Even though a 1-2 pixel error does not greatly affect performances, when considering non-overlapping blocks the impact of errors can increase. Excluding the case in which symmetrical errors happen, consider the following case in which the actual ground truth is still supposed to be 100:

0 0 0 0 1 0 0 1 1.

The procedure is here forced by the error to iterate between pixels 77 and 91, resulting in a predicted DKB of 91 if no further errors are made, or by a slightly lower value if an error occurs. Some observations are to be made: if the accuracy of the trained network is very high, errors are very unlikely to occur, this being even truer in the case of the reduced amount of predictions this procedure requests. It also has to be pointed out that it is preferable to have some rarer cases of error in the order of one centimeter than always applying a very computationally expensive algorithm. Furthermore, besides reducing the likelihood of an error, testing the network against a small number of samples for increasing r coordinates along the whole block provides a fast means of determining overall knots status, being the vector with all 0s an indicator of a globally sound knot.
Another important observation to be made regards the fact that, being the last examined sub-block centered around pixel 119, the final 8 pixels for each knot are never considered as block center: as already remarked in previous paragraphs, this does not greatly affect final product quality since they belong to an area in which most cutting patterns do not envisage the presence of any board.

Up to this point, only status estimation was concerned. But the change in perspective required by the employed dataset also regards diameter estimation: as the knowledge of actual DKB position was not strictly necessary (even if an estimate was nonetheless provided), so it is for diameter, which has only to be estimated at its intersection with boards. The attention is therefore shifted from knot diameter to diameter estimation at a certain coordinate.

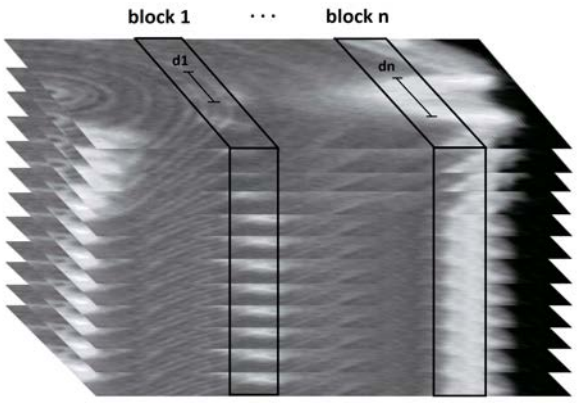

Figure 3.19: Representation of the (n) diameter samples available for a knot.

To do so, a slightly different procedure from the one adopted for DKB is followed: the CNN is trained with sub-block of the same size (i.e. 15 pixels wide along r), but this time no further blocks than the ones having a corresponding manual measurement are created. This is mainly because, even though an interpolation of inter-sample values could still be performed by following one of the existing knot models, such dataset adaptation could have a significant impact in reducing overall precision, since several sources of error, including imperfect measurements and models, are present.
For what regards the second part of the procedure, following network training, the same algorithm adopted for DKB can not once again be followed because of the different nature of the problem (classification vs regression). Since each diameter estimation requires the application of the CNN to a sub-block, it is envisaged that the application of this network is to be performed after the final cutting pattern has been chosen and knot status has been determined. Given that knot diameter plays a role in the determination of the best cutting option, too, this procedure could also be used as a refinement of an original estimate obtained by the application of some knot model for diameter estimation and used in cutting pattern selection.

3.2.4 Approach 4: estimation from sparse measurements and automatically extracted knot blocks (SMA)

Procedure and Dataset

The procedure defined in the description of the previous approach is employed in this last one as well, with the exact same CNN structure and algorithm working principles. It will be referred to as SMA, standing for *Sparse Measurements, Automatic*, where "automatic" refers to block extraction. Only a small, but significant, change in dataset construction occurs.
In the previous case, all knot blocks came from precise selections starting and ending point for each knot (in most cases even more than one middle point was selected), thus allowing for a close-to-perfect knot detection. Such tailored knot blocks are not always available in a real-life scenario, since some noise coming from the presence of other wood defects or other knots in close proximity of the one under consideration may slightly alter performances in the segmentation step performed after scanning.
The end point of a knot can, for instance, happen to be not exactly centered with respect to the t axis of the corresponding block, as reported in Figure 3.20.

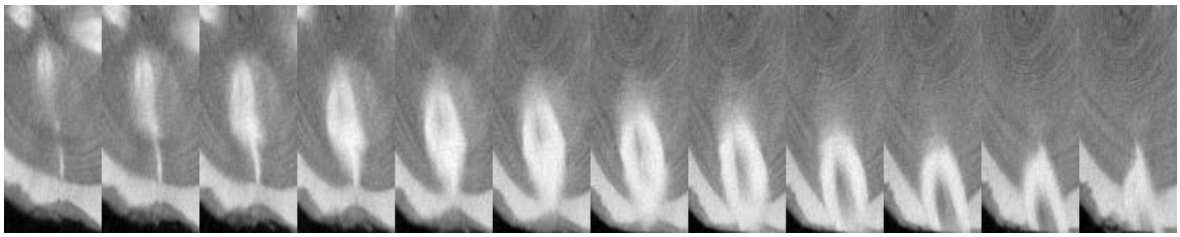

Figure 3.20: An automatically extracted knot block.

Even though this example is just slightly off-center, some worse cases are not too unlikely to be neglected and give further motivation to employ a slightly different dataset.
The most straightforward and effective way to face this problem is to employ in network

training the same block extracted after segmentation and employed in the first two approaches described in this work. Extracting such blocks is not enough, though, to perfect the procedure, since some decisions have to be made in order to determine how the position of manual measurements are to be reported to the reference system of each block.
This is necessary since, while in the previous case knot axis could be roughly assumed to be coinciding with the *r* one of the block since at least start and end point were aligned with it, now this assumption can no longer hold true for the reasons listed above. Such adaptation is performed as follows: the idea, which requires some adaptations to the software accompanying CT Log, is to keep track of *r* axis three-dimensional position while extracting each knot block, and to then make this information available when operating in the labeling software. Assuming, with more thin fair approximation, the starting point of the block to be in the pith and knowing its direction from the previous step, it is now possible to determine at which *r* coordinate each manually measured knot sample lies by operating the same two-steps procedure described in the previous subsection.

3.2.5 Summary of employed datasets

As explained in the introduction to section 3.2 and in the following paragraphs, several datasets with different constructions are employed in this work: this is mainly because of differences in the design of each approach lead to the need of a specific ground truth.
The network designed in DR is trained and tested on a previously existing dataset with manually-marked values for DKB and diameter; new blocks concerning sound knots are needed in SD, but the different block size provided in output by CT Log also leads to the need of obtaining new dead samples too, not allowing to re-employ blocks relative to CR.
SMS and SMA are based on a completely different paradigm and require an ad-hoc scanning procedure: while in the previous cases data was gathered from logs scanned in an actual sawmill application an later analyzed to create the necessary ground truths, stems employed in these two latter approaches were accurately marked and measured before scanning, and scanning itself was performed on a CT Log not operating in an in-line plant. The differ from one another only in knot block extraction (manually marked knots on a software for SMS, automatically extracted blocks for SMA) while referring to the exactly same logs and knots. A comparative table is here reported for further clarity.

Procedure	Goal	Ground Truth	Block Dimension	Available Data
DR	Diameter/DKB regression on whole blocks	CT	128 x 64 x 08	549 blocks
SD	Status Determination on whole blocks	CT	128 x 64 x 12	686 blocks
SMS	Status/DKB estimation on boards	Physical	128 x 64 x 12	634 blocks, 2412 samples
SMA	Status/DKB estimation on boards	Physical	128 x 64 x 12	634 blocks, 2412 samples

Table 3.1: A summary of employed datasets.

Chapter 4

Results

The whole developing and testing phases of the proposed methods, as well as time measurements (when reported) were performed on the same computer, running Windows 10 Pro on an Intel Core i7-4770, 3.4GHz processor and equipped with an Nvidia Geoforce RTX 2080 GPU. All the parts concerning neural networks were developed in python, by using the Keras 2.2.4 library on a Tensorflow 1.13.1 backend.

4.1 Approach 1: Direct Regression (DR)

While training all the three networks, the original set of 549 knots is thus split: 330 for training, 110 for validation and 109 for testing. Data augmentation consisting in flips along the l and t axis, separately, is performed, raising the total of training samples to 990.
The employed network structure, which is approximately the same utilized for results reported in the next sections with some obvious problem-related differences in the final layers, is rather simple: three equal convolutional blocks composed of two convolutional layers and a pooling one each, followed by a fully connected one. Adam optimizer is employed and mean squared error is the considered loss function.

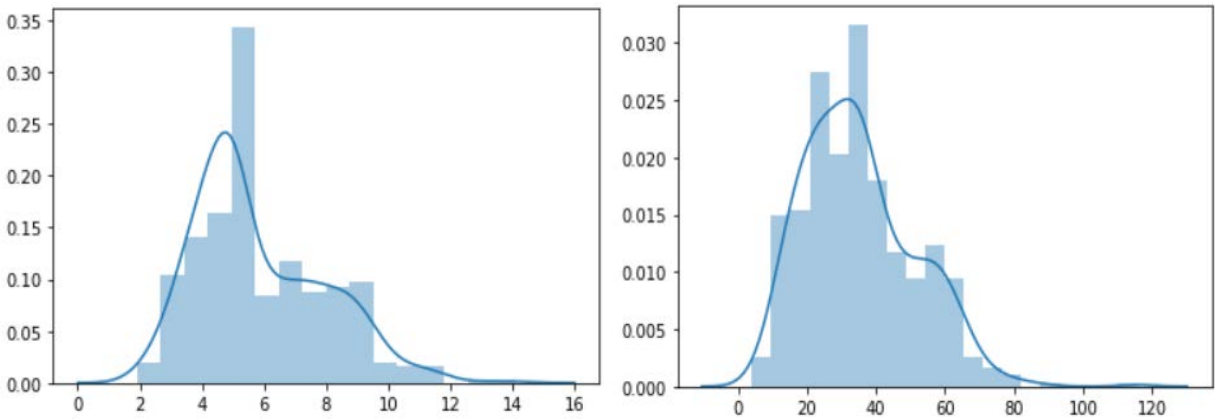

(a) Input diameter distribution.

(b) Input DKB coordinate distribution.

Figure 4.1: Input distributions.

Before proceeding with the description of obtained results, it seems necessary to comment the

distribution of input ground truth (see Figure 4.1), since it appears to bear some consequences to the output. The abscissa on the left reports diameter value in millimeters, while its correspondent on the right marks DKB coordinate in pixels. In this particular case, the distributions show how available knot samples are, in most cases, of reduced dimensions. DKB coordinate distribution is approximately centered around 35, but has a tail of some samples over 65, with a few outliers in the proximity or over 100.
Even though obtained on a dataset created by means of a software and not validated on physical ground truth, results yielded by the CNN on the test set appear to be quite promising: a mean error of 0.34 pixels for diameter with a 1.04 std, while corresponding values for DKB coordinate are 0.864 and 11.60 pixels.
Such results assume a slightly different value if further investigated, as the distribution of the errors reported in the following figure suggests.

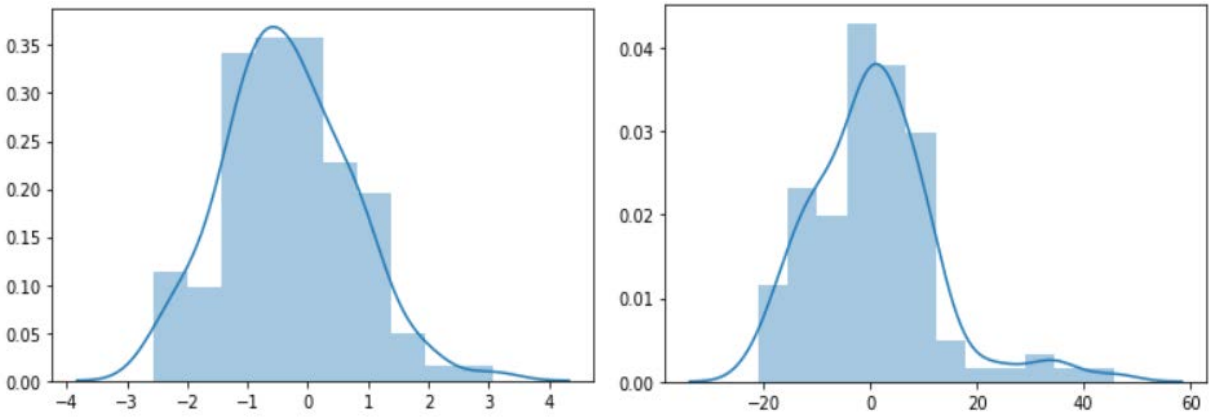

(a) Predicted diameter error distribution. **(b)** Predicted DKB coordinate error distribution.

Figure 4.2: Error distributions.

While diameter error distribution appears fairly symmetrical and seems to testify for the goodness of reported performances, the DKB one is strongly unbalanced towards higher values, showing the presence of errors in the estimation comprised between 20 and 44, which are quite high values if considering that the r axis only covers 128 pixels.
When more closely inspecting the cases in which the prediction remarkably differs from the corresponding ground truth, this most often happens for samples whose DKB lies in the tail of the distribution in Figure 4.1b, either implying that the network consistently underestimates DKB position and/or that too few samples with high DKB coordinates are available in the dataset.
The CNN regressing both parameters (procedure DR2, opposed to DR1 employing two different CNNs) at once obtained interesting performances: 0.0 *mm* mean error and 0.96 std for diameter, while 0.19 pixels mean error 10.06 std for DKB coordinate. Error distributions are reported in Figure 4.3, showing DKB in blue and diameter in orange. Results here are, clearly, slightly better (even though a couple of outliers are still present on the right hand side of the image) than the case with two separate networks: as the numbers indicate, diameter error distribution is narrower and more zero-centered, while the DKB coordinate one, even if still quite spread, presents fewer irregularities.
A possible interpretation of these results is that, since some correlation between the two quantities of interest undoubtedly exists, this fact eases the learning process during the training of

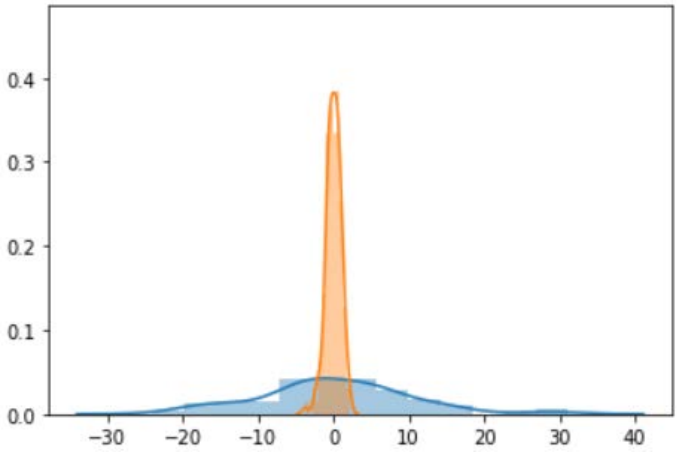

Figure 4.3: Predicted error distribution of diameter and DKB coordinate together.

the CNN, allowing to obtain slightly better results.
Anyway, in order to provide further evidence to this statement, additional tests involving a more complete dataset should be carried out.

4.2 Approach 2: Status Determination (SD)

Given that 343 sound Scots Pine knot samples are available, only 343 dead ones are considered for network training, to guarantee balancing between classes. Training, validation and test samples are 387, 128 and 171, respectively. Network structure and data augmentation are the same as the previous case, with an obvious difference in the loss function, being for this approach the binary cross-entropy one, since dealing with classification.
After several tests, the average reached accuracy on test set is 0.93.
The result alone is, in this case, of rather difficult interpretation: the non-negligible uncertainty in labeling training samples can result in the network still obtaining high accuracy with respect to the labels it was provided with, while these labels being consistently wrong because of an human error in the classification process (which is not totally unlikely given that it was carried out solely relying on CT images). Further tests are thus required to verify the goodness of achieved network performances.
For this reason, some simulations of the application of such network to entire logs, whose knots were not involved in the training and testing process, are run by properly adapting the software employed in log analysis. A ground truth coming from observation of real boards is not available in this case, too, but the information relative to knot position in the tree is accessible: a knot is, in fact, more likely to be sound if it is "large" if compared to log size and if it is placed in proximity of tree top, rather than in lower portions of it.
Under these assumptions, the CNN seems to achieve quite satisfactory performances, since consistently classifying as dead all knots not reaching log edge and most larger ones not respecting all the four points listed in Chapter 4. Moreover, classification appears to be slightly biased toward marking as sound knots reaching log edge: this is once again a desirable property, since any error is most likely to occur in the region closest to log edge, hardly ever included in sawn products.
Similar performances are achieved when running identical simulations on Maritime Pine logs.
Even though not directly acting on DKB coordinate estimation, this classification approach

still partially improves its performances, since previously employed algorithms failed in some cases to recognize fully sound knots and assigned them a DKB value, thus fitting products of worse quality in areas which are instead more valuable and so obtaining a sub-optimal product value.

4.3 Approach 3: Sparse Measurements, Software (SMS)

Out of the 13 Scots Pine log considered for this study, 634 knots are extracted, carrying a total amount of 2412 manual measurements on physical boards. Each knot has a variable number of samples referring to it, ranging from 1 up to, in a few cases 5 or 6.
Before training the network, a set of 158 knots, with a total of 549 relative manual measurements, are randomly chosen as test set both for validating network performances and for the testing phase aimed at estimating DKB coordinate. Therefore, for network training, 476 knot blocks and 1863 measurements, are employed.
In total, 46556 knot sub-blocks and the relative sound/dead labels are obtained: 12060 for testing (from the 158 knots mentioned above), 8624 for validation and 25872 for training.
The CNN, trained with a total of approximately 70000 samples after balancing between classes is guaranteed (data augmentation with t and l flips performed), reaches an accuracy of 95.9%. The final prediction, resulting after the estimation of a DKB coordinate according to the second part of the procedure described in subsection 3.2.3, yields a precision of 94.2% of correct status classification on knots coming from physical boards. The confusion matrix relative to this test is reported in Table 4.1.

		Predicted	
		Sound	Dead
Actual	Sound	230 (95.8%)	010 (04.2%)
	Dead	022 (07.1%)	287 (92.9%)

Table 4.1: Confusion matrix for SMS.

Even though such results may appear to be very promising, since current performances are estimated to be around 75%, it is necessary to recall that, in this approach, block coming from accurate manual definition of knot parameters are employed, instead of the ones resulting from automatic detection and extraction which are actually concerned in practical applications.
Since the main goal of SMS is to serve as preliminary test for DKB coordinate estimation algorithm to be employed in SMA, tests concerning diameter are not performed in this case.

4.4 Approach 4: Sparse Measurements, Automatic (SMA)

Since the dataset, for the part concerning manual measurements, is exactly the same as in the previous section, the split into training, validation and testing phases is very similar, with the only difference that this time the test set contains 577 measured samples, yielding a total of 11639 sub-blocks, while training and validation sets have 26188 and 8729 samples, respectively. After data augmentation and class balancing, a total of approximately 7100 training samples is available.

The network reaches an accuracy of 94.3% on the test set, while the final algorithm correctly classifies 86.5% of knot status on boards. The confusion matrix relative to this last result is reported in Table 4.2.

		Predicted	
		Sound	Dead
Actual	Sound	301 (88.5%)	039 (16.4%)
	Dead	039 (11.4%)	198 (83.5%)

Table 4.2: Confusion matrix for SMA.

A closer inspection to these results reveals that the decrease in performances with respect to the previous approach is due, besides to the lower accuracy brought in by the structure of input voxel blocks, by the fact that some few cases with large DKB estimation errors lead to more than one wrong status prediction on boards, since a single knot block may have several associated manually measured knots.
Some instances of knots with the relative DKB prediction marked as a white, horizontal line are reported in the following, starting from some instances of correct prediction in Figure 4.4. Besides the coordinate relative to DKB position, also the ones referring to the last sound measured sample and the first dead one are highlighted with a green and a red line, respectively.

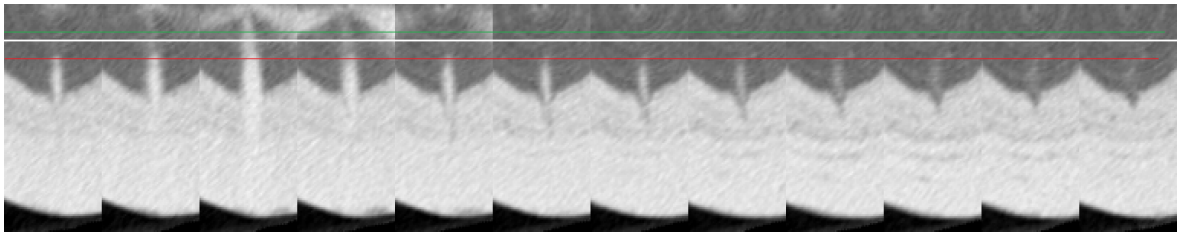

(a) Knot dying in proximity of the pith.

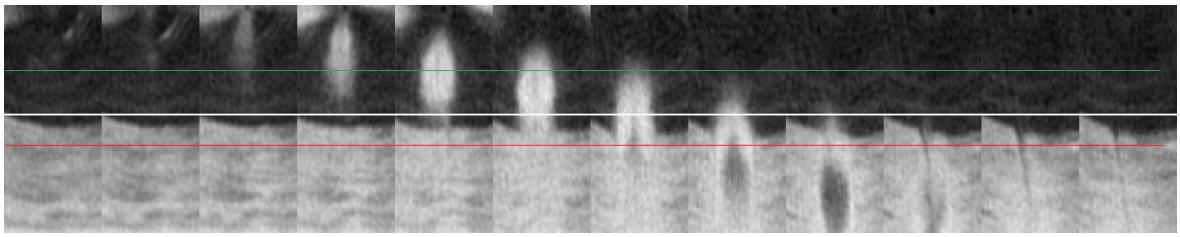

(b) Knot dying close to the heartwood-sapwood border.

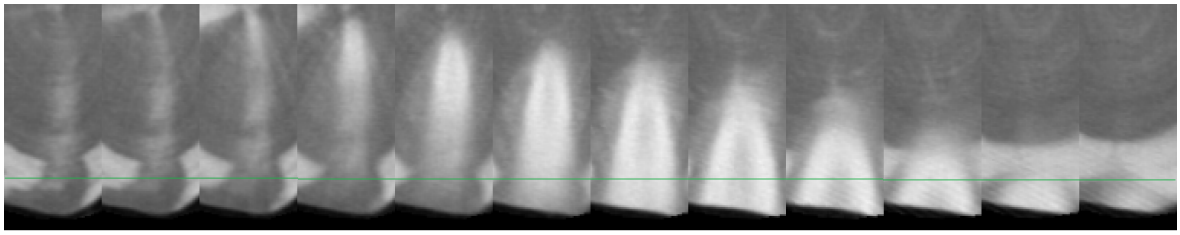

(c) Sound knot.

Figure 4.4: Some correct predictions.

Figure 4.4a and Figure 4.4b both report the case in which prediction falls in the desired area, i.e. the one where no sure information about knot status is available.
While, for the second figure, the standard criterion of marking as DKB the coordinate in which diameter stops growing would have allowed to perform a fairly correct estimate, it can be noticed how, in the first one, DKB coordinate is (correctly) placed by the algorithm very closely to the pith, while an human observer would have more likely, in absence of ground truth knowledge, provided an estimate lying at higher r coordinates than the red line, where we know the knot to be surely dead.
Figure 4.4c instead reports a correctly labeled sound knot: in this case no white line is visible since no DKB coordinate can be found. The last available measurement is reported in green, since referring to a sound intersection with a board.
Three images are reported for the case of correct prediction in order to point out how the algorithm is able to recognize the area in which the knot dies without dependence on the coordinate, i.e. without a bias, or even to distinguish whether a knot is, in its entirety, sound or not, which are tasks not yet accomplished by the previously described approaches or by other existing algorithms.
In Figure 4.5 two wrong predictions are reported, instead.

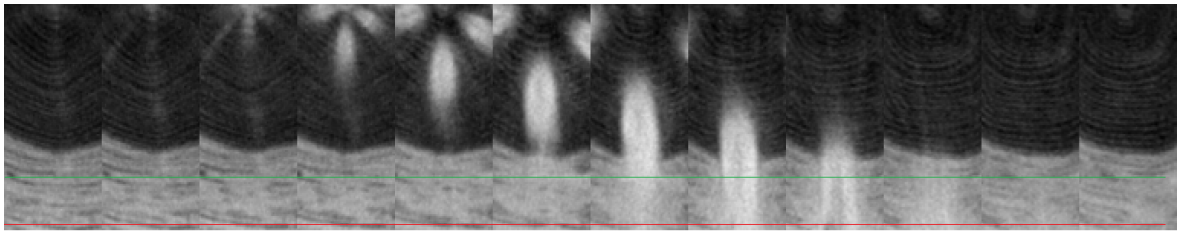

(a) DKB coordinate overestimated.

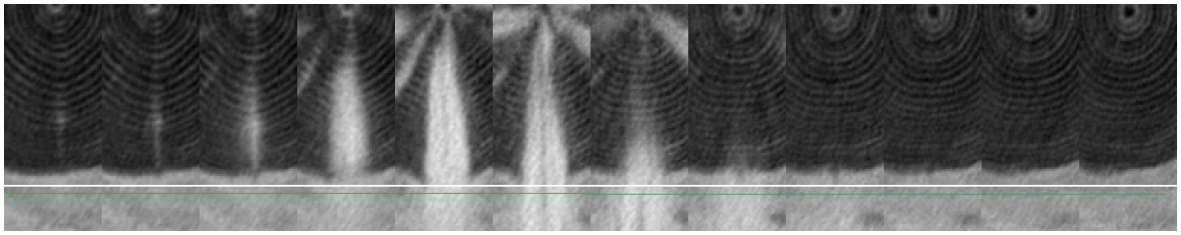

(b) DKB coordinate underestimated.

Figure 4.5: Two prediction errors.

More specifically, Figure 4.5a shows the case in which the knot is labeled as sound, but a dead sample is present in near coincidence of block end, and Figure 4.5b reports a block most likely containing completely sound knot (the last available sample is sound and close to log edge), where DKB is erroneously marked anyway.
Even though several of the errors, most likely due to the high but not excellent accuracy obtained by the CNN itself, concern the central r portion of knot blocks, a non-negligible share of them involves the sapwood area towards the end of the block.
This phenomenon, most likely due to the fact the network is trained on a range of samples not including the final few r coordinates and which are also not checked, for construction, by the algorithm, is again on one side negative and on the other acceptable: while the lack of precision can lead to some wrong classifications in the case of boards close to log edge, this is an area where few of them are fit.

Eventually, for what concerns performances, obtaining the prediction for a single sub-block (also including its extraction from the original knot block) requires about 0.42*ms* on average, leading to a total of 9 to 10 *ms* per knot.

For this last approach, results relative to diameter estimation are also available.
Only a sub-block per obtained measurement is employed in the procedure, thus leading to 2412 total samples for the training and testing of the network. One quarter of them is employed on the test set, and one quarter of the remaining is used for validation; the rest is left for training (1332 in total, without data augmentation).
On the test set, the CNN scores a mean error of -0.1*mm*, with a 3.2*mm* std.
A comparison between manual measurements and their prediction operated by the network is reported in Figure 4.6. As it can be seen, the measured R^2 is 0.827.

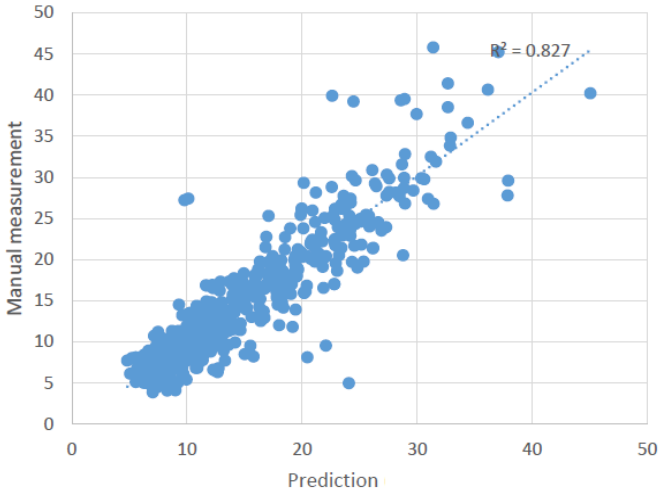

Figure 4.6: Comparison between measured and predicted knot diameters [36].

4.4.1 Summary

The following Table 4.3 reports a comparison between the designed procedures and the datasets they employ.

Procedure	Train/Val/Test samples	Training error/accuracy	Accuracy on boards
DR1, diameter	990/110/109	Mean: 0.34*px*, std: 01.04*px*	-
DR1, DKB	990/110/109	Mean: 0.86*px*, std: 11.60*px*	-
DR2, diameter	990/110/109	Mean: 0.00*px*, std: 00.96*px*	-
DR2, DKB	990/110/109	Mean: 0.19*px*, std: 10.06*px*	-
SD	1161/128/171	Accuracy: 0.930	-
SMS, status	25872/8624/12060	Accuracy: 0.959	0.942
SMS, diameter	-	-	-
SMA, status	26188/8729/11639	Accuracy: 0.943	0.865
SMA, diameter	26188/8729/11639	Mean: -0.1*mm*, std: 3.2*mm*	-

Table 4.3: A summary of employed datasets.

Obtained results appear to be rather good if compared with the ones reported at the end of Chapter 2. Table 4.4 and 4.5 below report an updated comparison with the algorithms available in the literature.

Paper	Performance
Johansson et al. [30]	mean error = $-4mm$, std = $12mm$
Oja [32]	$R^2 = 0.72$
DR2	mean error = $0.19px$, std = $10.06px$
SMS	acc. = 0.942
SMA	acc. = 0.865

Table 4.4: Updated comparison between performances on DKB estimation.

In the case of DKB coordinate estimation, results are again of difficult comparison: obtained results from DR are in pixel and of difficult conversion to mm (because the scale factor in r applied to input blocks was not available in this specific case, even if most often the dimension of a pixel is $1mm$ x $1mm$ since dealing with small logs, i.e. compression is not performed), but are quite similar to the ones obtained by Johansson et al., even if with lower mean error, while SMS and SMA are not comparable with other metrics. Anyway, the fact these results are obtained on physical measurements performed on real boards, alongside their rather high accuracy with respect to currently available performances testifies for their goodness.

Work	mean error [mm]	std [mm]	Scanner resolution [mm]
Longuetaud et al. [25]	0.67	3.28*	0.36-0.81 x 0.36-0.81 x 1.25
Longuetaud et al. [27]	0.0	0.9	0.74 x 0.74 x 3.75
Cool et al. [29]	-3.0	7.2	1.43 x 1.43 x 4.0
Friedriksson et al. [31]	-1.87	4.87	0.605 x 0.695 x 1.0
DR2	0.0	0.96	1.0 x 1.0 x 10
Oja 1997 [24]	2.6	2.2	n.a x n.a x n.a
Andreu and Rinnhofer [26]	0.7	10.1	1.55 x 1.55 x 20
Breinig et al. [28]	1.7	4.0*	1.0 x 1.0 x 1.1
Johansson et al. [30]	-0.93	4.6	n.a x n.a x 10
Oja 2000 [32]	-2.0	3.0	n.a x n.a x 10
SMA	-0.1	3.2	1.0 x 1.0 x 10

Table 4.5: Updated comparison between performances on knot diameter estimation.

Concerning diameter, results are again reported separately according to the way reference datasets were constructed.
While DR obtains comparable results with Longuetaud et al., but starting from lower resolution images, SMA achieves clearly better performances if confronted with the others.

Chapter 5

Conclusions

The goal of this work was to develop and test new techniques and algorithms to improve the automatic estimation of knot parameters in wood logs starting from tomographic images, under the constraint that such procedures are to be run in in-line sawmill applications and thus possibly lead to a trade-off between accuracy and computational efficiency.
Given that they are employed in many state-of-the-art techniques in the field of computer vision, CNNs are envisaged to be included in such procedures.
A brief introduction to tree biology and wood defect formation was provided, and the crucial role of knots, among other wood defects, in the determination of final product value was assessed. Furthermore, the importance of correct status and prediction and fairly accurate diameter estimation of knots on final boards, and the corresponding impact on sawn product were reported.
The performances of algorithms aimed at these two tasks available in the literature were discussed, marking the distinction between the ones employing datasets directly coming from manually-marked CT data and those obtained by measuring physical wood samples. The difficulty in obtaining sufficiently large and accurate datasets for DKB coordinate regression with such techniques was also underlined.
Once CT Log by Microtec, the scanner employed for obtaining data and performing some simulations object of this thesis, was introduced, four different approaches tackling the issues of DKB coordinate regression/status estimation and knot diameter regression were presented. Approaches 1 and 2 (DR and SD) rely on data marked directly on CT images, and aim at the direct regression of the parameters and to overall knot status estimation respectively, while approaches 3 and 4 (SMS and SMA) introduce a novel DKB position estimation algorithm relying on CNNs, which operate on sub-portions of CT voxel blocks relative to knots, with the only difference of being trained on two slightly differently constructed datasets.
Obtained results for the first two approaches are quite promising, with some caveats: while DR achieves results comparable with the best performing algorithms tested on datasets coming from measurements on CT images, even outperforming them if considering the slightly coarser employed scanner resolution, and is partially completed by SD for what concerns globally sound knots, it is important to remark that such performances are not obtained on actual measurements on physical wood samples and therefore are not fully reliable in terms on in-line applicability.
SMS and SMA, instead, provide a computationally efficient mean of obtaining reliable estimates of knot status and diameter on each virtual board before cutting, without performing any explicit estimation of overall knot soundness/blackness. Performances obtained by these

two methods are also more accurately evaluated, since the focus is shifted on the achieved precision on final sawn products, rather than on the accuracy in the estimation of global knot parameters. Anyway, only performances of SMA can be taken into account when dealing with in-line applications, since knot blocks in SMS are not automatically extracted, as it happens in real-case scenarios.

Some possible improvements are proposed, in the following, solely for SMS, being it the only one allowing for direct and reliable application in sawmills and also leaving more room for adjustments.
Concerning diameter estimation, the available number of samples could be increased by fitting measurements on subsequent boards to one of the existing knot models that can be found in the literature and then enlarging the training set by adding information about the areas between physical boards, otherwise not covered by measurements.
To obtain an even higher number of samples and to train the network on boards actually coming from a real-life scenario, and not from logs cut and measured for this precise purpose, thus leading to slightly different products than ones in sawmills, a further improvement would be to obtain knot measurements from an automatic board scanner to be placed right after CT Log and the sawing line. Such an approach would, anyway, require the development of a board-matching system capable to retrace every scanned board to its virtual correspondent in the data obtained by CT Log.
Eventually, another step concerning status prediction, too, is the inclusion of more than one species in the training and testing process, in order to provide for more training samples and to obtain higher robustness in the CNN output and more flexibility for the whole system.

Bibliography

[1] Food and Agriculture Organization of the United Nations (FAO). Global forest resources assesment, 2015.

[2] Food and Agriculture Organization of the United Nations (FAO). Global demand for wood products, 2008.

[3] Food and Agriculture Organization of the United Nations (FAO). Global forest products, facts and figures, 2016.

[4] Federico Giudiceandrea, Enrico Ursella, and Enrico Vicario. A high speed ct scanner for the sawmill industry. *Proceedings of the 17th international non destructive testing and evaluation of wood symposium. Sopron, Hungary: University of West Hungary*, 01 2011.

[5] E. Ursella, F. Giudiceandrea, and M. Boschetti. A fast and continuous ct scanner for the optimization of logs in a sawmill. In *8th Conference on Industrial Computed Tomography (iCT 2018) at Wels, Austria*, 02 2018.

[6] Michael Ramage, H Burridge, M Busse-Wicher, G Fereday, Thomas Reynolds, Darshil Shah, Guanglu Wu, Li Yu, P Fleming, Danielle Densley Tingley, J Allwood, Paul Dupree, PF Linden, and O Scherman. The wood from the trees: The use of timber in construction. 02 2017. doi: 10.17863/CAM.10386.

[7] Panshin A.J. Brown, H.P and C.C. Forsaith. *Textbook of Wood Technology, Volume I*. McGraw-Hill, 1949.

[8] Peter A Thomas. *Trees*. Cambridge University Press, 2014.

[9] T T Kozlowski. *Growth And Development Of Trees, Volume 1*. Physiological ecology. Academic Press, 1971. ISBN 9780124242012,0124242014.

[10] Carpenter Roswell D. Sonderman David L.and Rast Everette D. Jones, Martin J. *Defects in Hardwood Timber*, volume 678 of *Agriculture Handbooks*. United States Department of Agriculture, 1989.

[11] Woods whys: A sawyers lament. `https://northernwoodlands.org/articles/article/sawyers-lament`. Accessed: 2019-07-25.

[12] Kretschmann, David E. 2010. Mechanical properties of wood. Wood handbook : wood as an engineering material: chapter 5. Centennial ed. General technical report FPL ; GTR-190. Madison, WI : U.S. Dept. of Agriculture, Forest Service, Forest Products Laboratory, 2010: p. 5.1-5.46.

[13] J. M. Dinwoodie and Building Research Establishment. *Timber, its nature and behaviour*. E and FN Spon, 2 edition, 2000.

[14] Christina Foley. *Modeling the effects of knots in Structural Timber*. PhD thesis, Lund University, 2003.

[15] J. Bodig and B. A. Jayne. *Mechanics of wood and wood composites*. Van Nostrand Reinhold., 1982.

[16] Matti Niskanen and Olli Silven. Machine vision based lumber grain measurement. pages 408–411, 01 2007.

[17] David Kretschmann, Roland Hernandez, and John Walker. *Grading timber and glued structural members*, pages 339–390. 09 2006. doi: 10.1007/1-4020-4393-7_10.

[18] Martin Bacher. Comparison of different machine strength grading principles. *COST E53 Conference 29th-30th October, Delft, The Netherlands.*, 01 2008.

[19] Fred William Taylor, Francis G. Wagner, Charles W. McMillin, I. L. R. Morgan, and Forrest Frank Hopkins. Locating knots by industrial tomography. a feasibility study. 1984.

[20] Brian Funt and Edwin C. Bryant. Detection of internal log defects by automatic interpretation of computer tomography images. *Forest Products Journal*, 37, 01 1987.

[21] Stig Grundberg and Anders Grönlund. Feature extraction with the aid of an x-ray log scanner. In *Proceedings from the 3rd International Seminar/Workshop on Scanning Technology and Image Processing on Wood : Skelleftea, Sweden, Aug. 17 - 19, 1998*, number 1998:27 in Teknisk rapport / Lulea tekniska universitet, 1998. Godkänd; 1998; 20071210 (cira).

[22] M Samson. Modelling of knots in logs. *Wood Science and Technology*, 27:429–437, 09 1993. doi: 10.1007/BF00193865.

[23] Stig Grundberg, Anders Grönlund, and Ulla Grönlund. The swedish stem bank : a database for different silvicultural and wood properties. Technical Report 1995:31, Lulea University of Technology, Wood Science and Engineering, 1995. Godkänd; 1995; 20071211 (cira).

[24] Johan Oja. A comparison between three different methods of measuring knot parameters in picea abies. *Scandinavian Journal of Forest Research*, 12(3):311–315, 1997. doi: 10.1080/02827589709355415.

[25] Jean-Romain Roussel, Frederic Mothe, Adrien Krhäenbühl, Bertrand Kerautret, Isabelle Debled-Rennesson, and Fleur Longuetaud. Automatic knot segmentation in ct images of wet softwood logs using a tangential approach. *Computers and Electronics in Agriculture*, 104:46 – 56, 06 2014. doi: 10.1016/j.compag.2014.03.004.

[26] Jean-Philippe Andreu and Alfred Rinnhofer. Modeling of internal defects in logs for value optimization based on industrial ct scanning. 2003.

[27] Fleur Longuetaud, Frederic Mothe, Bertrand Kerautret, Adrien Krhäenbühl, Laurent Hory, Jean-Michel Leban, and Isabelle Debled-Rennesson. Automatic knot detection and measurements from x-ray ct images of wood: A review and validation of an improved algorithm on softwood samples. *Computers and Electronics in Agriculture*, 85:77–89, 07 2012. doi: 10.1016/j.compag.2012.03.013.

[28] Lorenz Breinig, Franka Brüchert, R Baumgartner, and Udo Sauter. Measurement of knot width in ct images of norway spruce (picea abies [l.] karst.)-evaluating the accuracy of an image analysis method. *Computers and Electronics in Agriculture*, 85:149–156, 07 2012. doi: 10.1016/j.compag.2012.04.013.

[29] Julie Cool, Magnus Fredriksson, and Stavros Avramidis. Knot detection in coarse resolution ct images of logs. In *International Wood Machining Seminar (IWMS-23) :*, 2017.

[30] Erik Johansson, Dennis Johansson, Johan Skog, and Magnus Fredriksson. Automated knot detection for high speed computed tomography on pinus sylvestris l. and picea abies (l.) karst. using ellipse fitting in concentric surfaces. *Computers and Electronics in Agriculture*, 96:238–245, 08 2013. doi: 10.1016/j.compag.2013.06.003.

[31] Magnus Fredriksson, Julie Cool, Isabelle Duchesne, and Denis Belley. Knot detection in computed tomography images of partially dried jack pine (pinus banksiana lamb.) and white spruce (picea glauca (moench) voss) logs from a nelder type plantation. *Canadian Journal of Forest Research*, 47, 03 2017. doi: 10.1139/cjfr-2016-0423.

[32] Johan Oja. Evaluation of knot parameters measured automatically in ct-images of norway spruce (picea abies (l.) karst.). *Holz als Roh und Werkstoff*, 58:375–379, 12 2000. doi: 10.1007/s001070050448.

[33] Alexander Katsevich. Improved exact fbp algorithm for spiral ct. In *Advances in Applied Mathematics 32.4.*, pages 681–697, 2004.

[34] Federico Giudiceandrea, Alexander Katsevich, and Enrico Ursella. A reconstruction algorithm is a key enabling technology for a new ultrafast ct scanner. *SIAM News*, 49:1, 11 2016.

[35] Andreas Rais, Enrico Ursella, Enrico Vicario, and Federico Giudiceandrea. The use of the first industrial x-ray ct scanner increases the lumber recovery value: case study on visually strength-graded douglas-fir timber. *Annals of Forest Science*, 74:1–9, 04 2017.

[36] Stefano Giovannini, Davide Boschetto, Enrico Vicario, Mauro Cossi, Andrea Busatto, Stefano Ghidoni, and Enrico Ursella. Improving knot segmentation using deep learning techniques. In *21st International Nondestructive Testing and Evaluation of Wood Symposium*, 2019. Accepted, in press.

[37] Federico Giudiceandrea, Enrico Ursella, Enrico Vicario, and Andreas Rais. Increasing the value of strength graded timber by industrial computer tomography. In *Wood conference in timber engineering, Vienna.*, 08 2016.